doi:10.1093/brain/awr165 Brain 2011: 134; 2339–2357 | 2339

BRAIN
A JOURNAL OF NEUROLOGY

Vascular endothelial growth factor is upregulated by L-dopa in the parkinsonian brain: implications for the development of dyskinesia

K. Elisabet Ohlin,[1] Veronica Francardo,[1] Hanna S. Lindgren,[1] Stephanie E. Sillivan,[2] Sean S. O'Sullivan,[3] Andrew S. Luksik,[4] Fair M. Vassoler,[4] Andrew J. Lees,[3] Christine Konradi[4,5,6] and M. Angela Cenci[1]

1 Basal Ganglia Pathophysiology Unit, Department of Experimental Medical Science, Faculty of Medicine, Lund University, BMC F11, 221 84 Lund, Sweden
2 Neuroscience Graduate Program, Vanderbilt University, Nashville, Tennessee, 37232, USA
3 Queen Square Brain Bank for Neurological Disorders and Institute of Neurology, University College, London, UK
4 Department of Pharmacology and Psychiatry, Vanderbilt University, Nashville, Tennessee, 37232, USA
5 Center for Molecular Neuroscience, Vanderbilt University, Nashville, Tennessee, 37232, USA
6 Kennedy Center for Research on Human Development, Vanderbilt University, Nashville, Tennessee, 37203, USA

Correspondence to: K. Elisabet Ohlin,
Department of Experimental Medical Science,
Lund University,
BMC F11,
221 84 Lund, Sweden
E-mail: elisabet.ohlin@med.lu.se

Correspondence may also be addressed to: M. Angela Cenci, E-mail: angela.cenci_nilsson@med.lu.se

Angiogenesis and increased permeability of the blood–brain barrier have been reported to occur in animal models of Parkinson's disease and L-dopa-induced dyskinesia, but the significance of these phenomena has remained unclear. Using a validated rat model of L-dopa-induced dyskinesia, this study demonstrates that chronic treatment with L-dopa dose dependently induces the expression of vascular endothelial growth factor in the basal ganglia nuclei. Vascular endothelial growth factor was abundantly expressed in astrocytes and astrocytic processes in the proximity of blood vessels. When co-administered with L-dopa, a small molecule inhibitor of vascular endothelial growth factor signalling significantly attenuated the development of dyskinesia and completely blocked the angiogenic response and associated increase in blood–brain barrier permeability induced by the treatment. The occurrence of angiogenesis and vascular endothelial growth factor upregulation was verified in post-mortem basal ganglia tissue from patients with Parkinson's disease with a history of dyskinesia, who exhibited increased microvascular density, microvascular nestin expression and an upregulation of vascular endothelial growth factor messenger ribonucleic acid. These congruent findings in the rat model and human patients indicate that vascular endothelial growth factor is implicated in the pathophysiology of L-dopa-induced dyskinesia and emphasize an involvement of the microvascular compartment in the adverse effects of L-dopa pharmacotherapy in Parkinson's disease.

Keywords: Parkinson's disease; levodopa; D1 receptors; neuroplasticity; angiogenesis; blood–brain barrier

Abbreviations: LID = L-dopa-induced dyskinesia; RNA = ribonucleic acid; VEGF = vascular endothelial growth factor

Received February 24, 2011. Revised May 17, 2011. Accepted June 5, 2011. Advance Access publication July 19, 2011

Introduction

Long-term treatment with L-dopa in Parkinson's disease provokes abnormal involuntary movements, referred to as L-dopa-induced dyskinesia (LID), in a majority of the patients (reviewed in Manson *et al*., 2006). Maladaptive brain plasticity produced by the combined effects of dopamine denervation and dopamine replacement therapy is attributed a key role in the development of LID, although the relative contribution of different potential mechanisms has not yet been established (reviewed in Calabresi *et al*., 2008; Cenci *et al*., 2009; Voon *et al*., 2009).

Brain plasticity is not limited to neurons, but also involves astrocytes and microvascular cells forming the so called 'neurovascular unit', which undergo long-lasting functional and structural adaptations in a number of neurological diseases (Perea *et al*., 2009). Endothelial proliferation, angiogenesis and an ensuing transient increase in blood–brain barrier permeability can occur in the adult brain either as an adaptation to locally increased metabolic demands (Black *et al*., 1990; Swain *et al*., 2003; Ding *et al*., 2006) or as a response to injury (Cavaglia *et al*., 2001; Nag *et al*., 2002).

Post-mortem investigations on human Parkinson's disease brains and animal models of Parkinson's disease have provided evidence of angiogenesis in the substantia nigra pars compacta (Faucheux *et al*., 1999; Barcia *et al*., 2005; Carvey *et al*., 2005; Wada *et al*., 2006), which have attributed this phenomenon to the ongoing neurodegenerative and neuroinflammatory changes in this region. Increasing evidence, however, indicates that the pharmacotherapy of Parkinson's disease may have angiogenic effects on the brain microvasculature (reviewed in Cenci *et al*., 2009). Strong evidence of treatment-induced angiogenesis has been obtained in rats with unilateral 6-hydroxydopamine lesions treated chronically with L-dopa. Animals that develop abnormal involuntary movements in response to L-dopa exhibit endothelial proliferation, upregulation of immature endothelial markers (nestin), downregulation of blood–brain barrier proteins (endothelial barrier antigen) and parenchymal accumulation of albumin in the striatum and its projection targets (Westin *et al*., 2006; Lindgren *et al*., 2009). This angiogenic activity is restricted to the hemisphere ipsilateral to the 6-hydroxydopamine lesion, thus requiring a concurrence of dopamine denervation and chronic L-dopa treatment to be expressed. Pharmacological studies have shown that this angiogenic response is dependent on a stimulation of dopamine D1 receptors and extracellular signal-regulated kinases 1 and 2 (ERK1/2), and that it is opposed by dopamine D2 receptor stimulation (Lindgren *et al*., 2009). The angiogenic cytokines mediating endothelial proliferation and microvascular remodelling in this animal model are still unknown and a possible contribution of angiogenesis to the development of LID has not been proven.

In the present study, we have examined the expression of vascular endothelial growth factor in the parkinsonian brain and its possible role in the development of LID in the rat. Within the family of vascular endothelial growth factors (comprising VEGF-A, -B, -C and D), VEGF-A (hereafter referred to as VEGF) has the most potent angiogenic activity and is the predominant form in the brain (Ferrara *et al*., 1999; Rosenstein *et al*., 2004). VEGF is essential for vasculogenesis and for the sprouting of new capillaries during development (Carmeliet *et al*., 2000). It exerts a potent mitogenic effect on endothelial cells and can directly augment the permeability of the blood–brain barrier by regulating the expression of matrix metalloproteases and endothelial tight junction proteins (Bauer *et al*., 2010; Hawkins *et al*., 2010). The VEGF receptor 2 (VEGFR2) tyrosine kinase, also known as flk-1, mediates most of the angiogenic effects of VEGF (endothelial cell proliferation, chemotaxis and survival) via activation of intracellular signalling cascades (Larrivee and Karsan *et al*., 2000), among which ERK1/2 play an important role (Mani *et al*., 2003). VEGF is upregulated in the brain following traumatic injury, ischaemia or epileptic seizures (Rosenstein *et al*., 1998; Nag *et al*., 2002; Croll *et al*., 2004; Rigau *et al*., 2007; Nicoletti *et al*., 2008). This response can be viewed as both protective and potentially harmful because, while increasing tissue vascularization, VEGF also induces blood–brain barrier leakage and inflammation (Zhang *et al*., 2000; Krum *et al*., 2002). Functional links between dopamine receptor stimulation and VEGF signalling have so far been studied in endothelial cells and endocrine organs, where D2 receptor stimulation has been found to negatively modulate VEGFR2 tyrosine kinase phosphorylation and inhibit angiogenesis (Basu *et al*., 2001; Cristina *et al*., 2004; Sarkar *et al*., 2004; Gomez *et al*., 2006). The effects of dopaminomimetic treatments on the expression and function of VEGF in the brain have not, however, been addressed in any previous study.

Using a validated rat model of LID, this study provides the first demonstration that VEGF is induced by L-dopa treatment in the same basal ganglia nuclei that show histological evidence of angiogenesis. The protein is abundantly expressed in astrocytes and astrocytic end-feet apposed to microvessels. This response is causally linked with the development of abnormal involuntary movements, as indicated by the antidyskinetic effect of a small molecule inhibitor of VEGFR2, which also inhibits L-dopa-induced angiogenesis. We also provide evidence of angiogenic activity and upregulation of VEGF messenger RNA in post-mortem basal ganglia tissue from patients with Parkinson's disease having a history of LID.

Materials and methods

All experimental procedures on animals or human tissue were approved by the responsible ethical authorities at the host universities.

Experimental design for the rat studies

Three *in vivo* experiments using the rat model of LID were performed in this study (Fig. 1). Experiment 1 addressed the relationship between angiogenesis and drug dosage during chronic L-dopa treatment. Experiment 2 evaluated the expression of VEGF in response to the same L-dopa treatment regimens as in Experiment 1. Experiment 3 assessed the antidyskinetic and antiangiogenic effects of the VEGFR2 tyrosine kinase inhibitor, vandetanib (ZD6474; Astra Zeneca; Wedge *et al*., 2002) co-administered with L-dopa.

Figure 1 Experimental design of *in vivo* rat studies. The effects of L-dopa treatment on immunohistochemical indices of angiogenesis (Experiment 1), and on the levels of VEGF protein (Experiment 2) were studied using two dosing regimens ('high dose', 25 mg/kg, and 'low dose', 6 mg/kg given twice daily in combination with 12 mg/kg benserazide). The effects of the VEGFR2 antagonist, vandetanib (30 mg/kg/day) on dyskinesia and angiogenesis were studied in Experiment 3. All treatments were performed on rats with unilateral 6-hydroxydopamine lesions. ELISA = enzyme-linked immunosorbent assay; IHC = immunohistochemistry.

Animals and dopaminergic lesion

All drugs used for surgery were purchased from Apoteksbolaget AB. Female Sprague Dawley rats (225 g body weight on purchase; Harlan) were housed in a 12 h light/dark cycle with *ad libitum* access to food and water. 6-Hydroxydopamine lesion surgery was performed under anaesthesia with a 20:1 mixture of Fentanyl® and Domitor® injected intraperitoneally (i.p.). The 6-hydroxydopamine toxin was dissolved in 0.02% ascorbate/saline to a concentration of 3.5 μg/μl, and injected at the volumes of 2.5 μl and 2.0 μl at the following two coordinates (in millimetres, relative to bregma and the dural surface): (i) anteroposterior (AP), +4.0; lateral (L), +0.8; dorsoventral (DV), −8.0 (tooth bar, +3.4); and (ii) AP, +4.4; L, +1.2; DV, +7.8 (tooth bar, −2.4). Antidote and analgesia were given postoperatively [Antisedan® and Temgesic® subcutaneously (s.c.)]. Two weeks post-surgery, the animals' turning behaviour was recorded in an automated rotometre during a 90 min period following an injection of dexamphetamine (2.5 mg/kg; i.p.). Inclusion criteria for rats in the study were >5 net ipsilateral turns/minute, corresponding to >90% striatal dopamine denervation (Winkler *et al*., 2002). The lesion extent was finally verified by tyrosine hydroxylase immunohistochemistry.

Drug treatments

Chronic treatment with L-dopa and benserazide (i.p.) was initiated 3 weeks after the rotational screening, and lasted for 14 or 22 days (Fig. 1), as in our previous studies (Westin *et al*., 2006; Lindgren *et al*., 2009). Rats in Experiments 1 and 2 were treated bi-daily with a low dose (6 mg/kg) or a high dose (25 mg/kg) of L-dopa methyl ester combined with 12 mg/kg/day benserazide hydrochloride (Sigma Aldrich, AB). At the higher dose, all lesioned rats develop severe dyskinesia, while the lower dose leaves a proportion of the animals free from abnormal involuntary movements (Lindgren *et al*., 2007; Picconi *et al*., 2008). Control 6-hydroxydopamine lesioned animals received daily injections of physiological saline (0.9% NaCl, s.c.). In Experiments 1 and 3, rats received bi-daily injections of bromodeoxyuridine (50 mg/kg, i.p.) during the last 3 days of L-dopa treatment in order to label proliferating cells as in Lindgren *et al*. (2009). In Experiment 3, rats were co-treated with L-dopa and the high-affinity VEGFR2-antagonist vandetanib (30 mg/kg; maximum tolerated dose for chronic use) or its vehicle (1% Tween-80 in deionized water), given by oral gavage 4 h prior to each L-dopa/benserazide or saline injection, to reach a stable concentration in the brain during the duration of the L-dopa effect (Wedge *et al*., 2002; Gustafson *et al*., 2006). Because the induction of VEGF and angiogenesis by L-dopa is a dose-dependent phenomenon (see 'Results' section), the effects of the VEGFR2 antagonist were examined using an incremental dose regimen of L-dopa, consisting of 6 mg/kg (Days 1–12), 12 mg/kg (Days 13–17) and 24 mg/kg (Days 18–22). Half of the saline-treated rats ($n = 12$ in total) received vandetanib (30 mg/kg) and the other half received vehicle (1% Tween-80). These two groups were then pooled into one single control group since their behavioural and histological data were indistinguishable. Weights of the animals were monitored throughout the treatment period and no difference was found between vandetanib- or vehicle-treated rats.

Behavioural assessments

Abnormal involuntary movements were monitored by observation of each rat for 1 min every 20 min post L-dopa injection until the drug effect had subsided (180 or 240 min, depending on the drug dose). Axial abnormal involuntary movements (dystonic posturing or twisting movements of the neck and upper body towards the side contralateral to the lesion), limb abnormal involuntary movements (purposeless movements of the contralateral forelimb), orolingual abnormal involuntary movements (empty jaw movements and contralateral tongue protrusion) were scored on two severity scales graded from 0 to 4, i.e. the original scale by Cenci *et al*. (1998), which is based on the proportion of observation time during which dyskinesia is present, and an amplitude scale that is based on the degree of translocation of the affected body part and number of muscle groups involved (Cenci and Lundblad, 2007). A global abnormal involuntary movement score was obtained by summing the products of basic score and amplitude score for each dyskinesia subtype from each monitoring period as described in Lindgren *et al*. (2010).

The cylinder test of forelimb use asymmetry (Schallert *et al*., 2000) was used to assess the anti-akinetic effect of L-dopa as administered alone or together with the VEGFR2 antagonist vandetanib (Experiment 3). Each rat was placed in a glass cylinder, and the number of full appositions of the left and right forepaws to the cylinder wall was counted during a 3 min observation period (Lundblad *et al*., 2002). The cylinder test was performed on Days 7 and 14 of the chronic drug treatment period both at baseline (OFF L-dopa) and 90-min post-L-dopa injection (ON L-dopa).

Post-mortem human brain tissue and neuropathological investigations

Paraffin-embedded sections through the post-commissural part of the basal ganglia (including posterior putamen, internal and external segment of the globus pallidus), corresponding to levels 8 and 9 in the human brain atlas (Mai and Paxinos, 2004), were provided by the Queen Square Brain Bank for Neurological Disorders, London. The cases included neurologically healthy individuals (controls, $n = 6$), and 20 pathologically verified Parkinson's disease cases, divided into a dyskinetic group ($n = 11$) and a non-dyskinetic group ($n = 9$) based on clinical case records of LID. The groups were matched for age at death, post-mortem delay and tissue pH. Parkinson's disease groups were matched for age at disease onset, disease duration and duration

of L-dopa pharmacotherapy (Table 1). The neuropathological diagnosis of Parkinson's disease was based on severe depletion of neurons in the substantia nigra pars compacta associated with Lewy bodies in surviving nigral neurons (Gibb and Lees, 1988). Staging of Lewy body pathology (McKeith *et al*., 1996) and Alzheimer disease-like pathology (Braak and Braak, 1991) did not disclose any significant difference between dyskinetic and non-dyskinetic Parkinson's disease cases. In addition, we verified the extent of putaminal dopamine denervation using dopamine transporter autoradiography (Little *et al*., 1995; Huot *et al*., 2010) in the cases from which fresh-frozen basal ganglia sections were made available ($n = 8$ in each Parkinson's disease group, $n = 5$ in the control group). This analysis showed similar levels of dopamine transporter radioligand binding in dyskinetic and non-dyskinetic patients (12.3 ± 1.7 and $10.5 \pm 1.8\%$ of control values, respectively; *t*-test, $P = 0.5$).

Tissue samples for analysis of VEGF messenger RNA expression were collected at the Harvard Brain Tissue Resource Centre at McLean Hospital, Harvard Medical School, (HBTRC; http://www.brainbank.mclean.org). A round sample, ~2–3 mm thick, was taken in the mid-putamen from a coronal slice of the brain at the level of the optic chiasm. Clinical diagnosis was verified in the other hemisphere through neuropathological analysis, including semi-quantitative scoring of the degree of de-pigmentation (pallor) in the substantia nigra and locus coeruleus, microscopic examination of brainstem sections stained with conventional histological methods and staging of Alzheimer's disease-like pathology (Braak and Braak, 1991). Among all the parameters examined, the only one differing between dyskinetic and non-dyskinetic cases were the degree of substantia nigra depigmentation that was larger in the former group (score of 3.7 ± 0.14 versus 2.6 ± 0.21, respectively, on a scale from 0 to 4, $P = 0.005$). All medical records were examined for any symptoms attributable to LID, under observation of all Health Insurance Portability and Accountability Act (HIPAA) and Institutional review board guidelines and with a questionnaire developed by the investigators (Naydenov *et al*., 2010). Because the number of female samples with complete medical records was small and uneven across the groups, analyses were restricted to males (Table 2). Investigators were blinded to the diagnosis.

Tissue preparation and immunohistochemistry of rat sections

Rats received a terminal dose of sodium pentobarbital (50 mg/kg) 18 h after the last L-dopa/saline injection as in Konradi *et al*. (2004) and Westin *et al*. (2006). Animals were transcardially perfused with 50 ml 0.9% NaCl and 250 ml ice-cold 4% paraformaldehyde in 0.1 M phosphate buffer. For free-floating immunohistochemistry, brains were post-fixed for 2 h in paraformaldehyde, transferred to 25% sucrose solution in 0.1 M phosphate buffer for cryoprotection and sectioned coronally on a freezing microtome (40 μm thick). For paraffin embedding, brains were dehydrated in increasing concentrations of alcohol to xylene, followed by changes of hot paraffin wax and embedding. Sections were cut at a thickness of 5 μm and dried overnight at 37°C.

Free-floating immunohistochemistry was performed as previously described (Westin *et al*., 2006). Endogenous peroxidases were quenched using 3% H_2O_2 and 10% methanol for 20 min. Sections were incubated in 0.02 M potassium–phosphate buffered saline with 0.1% Triton-X (KPBS/T) and blocked in a solution of 5% normal serum (1 h). All primary antibodies were incubated at 4°C in KPBS/T containing 5% normal serum, and secondary antibodies in KPBS/T with 2.5% normal serum (see Table 3 for detailed information regarding primary and secondary antibodies). Detection of antibody complexes was performed using either a peroxidase-based method (with 3′3′-diaminobenzidine as the chromogen) or conjugated fluorophores. Slide-mounted sections were coverslipped with DPX mounting medium or polyvinyl alcohol-1,4-[2.2.2]-octane, respectively (Sigma-Aldrich, AB).

VEGF immunohistochemistry was performed on paraffin-embedded sections after having established that this method of tissue preparation yielded superior morphological detail (particularly for neuropil staining). We used a well-characterized primary antibody (Table 3) (Tran *et al*., 2005; Wada *et al*., 2006; Nicoletti *et al*., 2008), whose specificity was further verified by pre-absorption of the primary antiserum with the corresponding immunizing peptide (Santa Cruz Biotechnology, sc-152-P) according to manufacturers' recommendations. Sections were deparaffinized in xylene followed by

Table 1 Sample demographics and clinical data for the human cases used for histology

Values (mean ± SEM)	Healthy controls	Non-dyskinetic Parkinson's disease	Dyskinetic Parkinson's disease	*P*-value (statistical test used)
n	6	9	11	
Male: Female	4:2	6:3	5:6	0.6 (Chi-square)
Age of death	79.4 ± 4.7	74.6 ± 3.0	76.3 ± 1.9	0.6 (ANOVA)
Post-mortem delay (h)	50 ± 10	42 ± 7	49 ± 7	0.7 (ANOVA)
Tissue pH	6.3 ± 0.1	6.4 ± 0.1	6.4 ± 0.1	0.7 (ANOVA)
Age at Parkinson's disease onset (years)	NA	60.6 ± 4.3	59.0 ± 2.5	0.8 (*t*-test, $t = 0.3$)
Parkinson's disease duration (years)	NA	14.0 ± 2.5	17.3 ± 1.9	0.3 (*t*-test, $t = -1.0$)
Maximum L-dopa dose (mg/day)	NA	536 ± 84	695 ± 67	0.2 (*t* test, $t = -1.5$)
Years of L-dopa use	NA	10.9 ± 2.1	14.7 ± 2.0	0.2 (*t* test, $t = -1.3$)
Lifetime L-dopa amount (g)	NA	2055 ± 664	2700 ± 338	0.4 (*t*-test, $t = -0.9$)
Years of any dopamine agonist use	NA	1.4 ± 0.7	4.6 ± 1.1	0.03 (*t*-test, $t = -2.4$)
Months of Parkinson's disease without dyskinesia	NA	168.5 ± 30.1	71.8 ± 13.2	0.013 (*t*-test, $t = 2.9$)
Months of L-dopa use without dyskinesia	NA	132.0 ± 25.4	41.0 ± 8.0	0.007 (*t*-test, $t = 3.4$)

NA = not applicable.

Table 2 Sample demographics and clinical data for human cases used in the quantitative polymerase chain reaction analysis of VEGF

Values (mean ± SEM)	Healthy controls	Non-dyskinetic Parkinson's disease	Dyskinetic Parkinson's disease	*P*-value (statistical test used)
n (all male)	18	12	11	
Age at death	72.2 ± 7.9	74.3 ± 5.0	75.9 ± 7.3	0.3 (ANOVA)
Post-mortem delay (h)	16.4 ± 4.8	16.4 ± 6.0	15.0 ± 5.2	0.9 (ANOVA)
Age at Parkinson's disease onset (years)	NA	68.2 ± 7.7	57.8 ± 8.9	0.6 (*t*-test, $t = -2.7$)
Parkinson's disease duration (years)	NA	7.8 ± 5.1	16.5 ± 8.4#	0.02 (*t*-test, $t = 2.8$)
Years of L-dopa use	NA	4.0 ± 3.3	10.2 ± 5.6	0.1 (*t*-test, $t = 2.7$)
Lifetime L-dopa amount (g)	NA	768.8 ± 965.5	2707 ± 2436#	0.004 (*t*-test, $t = 2.3$)
VEGF messenger RNA levels/normalization controls (average of the two primers used)	0.865 ± 0.085	0.967 ± 0.157	1.475 ± 0.233*,#	0.016 (ANOVA)

NA = not applicable.
*$P < 0.05$ vs healthy controls, # versus non-dyskinetic Parkinson's disease patients.

Table 3 Primary and secondary antibodies used in the histological analyses

Antibody	Dilution	Incubation time	Source	Marker of	Application
Primary antibodies					
Rabbit-anti-tyrosine hydroxylase	1:1000	Overnight	Pel-Freeze, Rogers, AR, USA	Tyrosine hydroxylase Dopaminergic neurons	Rat IHC, FF
Rat-anti-BrdU	1:100	36h	Serotec, UK	Proliferating cells	Rat IF, FF
Rabbit-anti-laminin	1:100	36h	Sigma-Aldrich, Sweden	Endothelial basal lamina	Rat IF, FF
Mouse-anti-nestin	1:5000	Overnight	BD Pharmingen,	Immature endothelium	Rat IHC, FF
Sheep-anti-albumin	1:60000 1:5000	Overnight	Biogenesis, USA	Albumin extravasation	Rat IHC, FF Human IHC, PF
Mouse-anti-endothelial barrier antigen (EBA)	1:1000	Overnight	Covance, USA	Endothelium with intact BBB properties	Rat IHC, FF Rat IF, PF
Rabbit-anti-VEGF (A-20)	1:30 1:100	Overnight	Santa Cruz, USA	Vascular endothelial growth factor (VEGF)	Rat IF/IHC PF Human IHC, PF
Mouse-anti-GFAP	1:100	Overnight	Millipore	Glial fibrillary acidic protein, astrocytes	Rat IF, FF/PF
Mouse-anti-CD11b (OX-42)	1:100	Overnight	Serotec, UK	Microglia	Rat IF, FF
Mouse-anti-CD68 (ED-1)	1:100	Overnight	Serotec, UK	Activated microglia	Rat IF, FF
Mouse-anti-CD34	1:300	Overnight	Serotec, UK	Endothelium	Human IHC, PF
Mouse-anti-human nestin	1:750	Overnight	Millipore	Immature endothelium	Human IHC, PF
Secondary antibodies					
Biotinylated-goat-anti-rabbit/ Biotinylated-horse-anti-mouse	1:200	2 h	Vector Laboratories		Rat IF, FF / Human IHC, PF
Cy3-donkey-anti-rat Cy2/ Cy3-donkey-anti-mouse (IgG and IgM specific, respectively) Cy5-donkey-anti-mouse	1:200	2 h	Jackson Immunoresearch		Rat IF, PF, FF

BBB = blood brain barrier; BrdU = bromodeoxyuridine; FF = free-floating; IF = immunofluorescence; IHC = bright-field immunohistochemistry; PF = paraffin-embedded sections.

decreasing concentrations of alcohol (100–70%) and rinsed in distilled water. Heat-induced epitope retrieval was performed in Tris–base (pH 10) for 15 min in a microwave oven (700 W). Sections were pre-incubated in blocking solution and incubated with primary antibodies as described above (Table 3). Visualization was performed using the diaminobenzidine method, followed by 2 min immersion in Mayer's haematoxylin to obtain a nuclear counterstain. Triple immunofluorescence was achieved using species- and immunoglobulin-specific fluorophore-conjugated secondary antibodies (Table 3).

Tissue preparation and immunohistochemistry of human sections

After fixation in 10% buffered formalin, post-mortem brains were paraffin embedded, from which 7-μm thick sections were cut and mounted on Histobond-coated slides. Sections for immunohistochemistry were prepared using the same procedure as for the rat sections

(see above). Sections were pre-incubated with 2% normal serum in Tris-buffered saline containing 0.25% Triton-X (TBS-T) for 30 min, and incubated with the primary antibody (Table 3) followed by species-specific biotinylated secondary antibodies (both in 1% normal serum/TBS-T). Immunocomplexes were visualized with diaminobenzidine. All sections were then counterstained with Mayer's haematoxylin. In addition, sections used for quantitative image analysis (CD34 and nestin) were counterstained with Luxol Blue (overnight at 37°C) to allow for an exact delineation of the structures of interest.

Cell counts and image analysis

Quantitative image analyses were carried out by an experimentally blinded investigator. In the rat studies, all analyses included three sections per animal/marker/structure at a relative inter-distance of 240 μm, covering the mid-caudal striatum and mid-caudal substantia nigra pars reticulata, respectively, according to our established procedures (Westin *et al*., 2006). Manual counts of double-labelled bromodeoxyuridine/laminin cells were performed using a Nikon Ecplise 80i microscope with a ×40 objective, equipped with a dual fluorescence filter and a grid providing a sampling frame of 0.25 × 0.25 mm. Nestin- and endothelial barrier antigen-immunopositive microvessels were quantified using the image segmentation software VIS (Visiopharm Integrator System; Visiopharm) by a method thoroughly described in Westin *et al*. (2006). Briefly, images were captured bilaterally in each structure with a digital camera (Olympus DP72). On each image, the immunopositivity associated with blood vessels was separated from light and dark background using a Bayesian algorithm-based pixel classifier. In the substantia nigra pars reticulata, images were captured with a ×4 objective to include the entire structure, while striatal areas were sampled under the ×10 objective to cover the lateral half of the striatum. The extent of parenchymal albumin extravasation was assessed by capturing images on a light table with constant illumination using a digital camera (Nikon DXM1200F) followed by densitometric analysis of 8-bit images using ImageJ software (Version 1.32j, NIH). Confocal microscopic analysis was performed on sections processed for dual- or triple-antigen immunohistochemistry using a LSM510 Laser Scanning Microscope (Carl Zeiss).

Quantification of microvessel-associated CD34 and nestin immunostaining on paraffin-embedded human sections were carried out with a Nikon Ecplise 80i microscope equipped with an automated stage. Briefly, each structure of interest was encircled in a mask at ×4 magnification. Within each mask, a systematic random sampling was applied using the VIS software so as to cover a fixed percentage of the structure of interest (2% in the putamen, 3% in each external globus pallidus and internal globus pallidus). Sample areas of each frame (0.024 mm^2) were captured with a random orientation using a ×20 objective, obtaining 20–60 areas per patient and structure (depending on the total size of the section). The total size of each structure did not significantly differ between the groups (compared by one-way ANOVA). Images were analysed using threshold analysis distinguishing vessels as opposed to tissue background using the VIS software. Results were expressed as the total number of immunopositive pixels per unit area (mm^2).

Enzyme-linked immunosorbent assay

For experiments analysing VEGF protein levels with enzyme-linked immunosorbent assay, rats were euthanized 6 h after the last L-dopa injection, an interval sufficient to detect upregulation of VEGF protein in the brain (Marti *et al*., 2000; Mani *et al*., 2003; Nicoletti *et al*., 2008; Schmid-Brunclik *et al*., 2008). Brains were removed from the skull and immersed into isopentane (−70°C in dry ice). Dissection of the dorsolateral striatum and substantia nigra pars reticulata was performed in a cryostat at −18°C (see Supplementary Fig. 1 for a detailed description). Tissue was homogenized by sonication in ice-cold 0.15 M phosphate buffered saline containing 1% Triton-X, 0.1% sodium dodecyl sulphate, 0.5% sodium deoxycholate and protease inhibitors (ROCHE complete, ROCHE diagnostics). The homogenate was centrifuged for 10 min at 4°C. The supernatant was used for further analysis. The enzyme-linked immunosorbent assay reaction for VEGF (mouse VEGF Quantikine kit, R&D systems) was made on duplicate samples of 50 μl of homogenate according to the manufacturers' instructions. The luminometric reaction was quantified using a spectrophotometer (ElX800™, BioTek instruments) at 450 nm with correction wavelength 550 nm. Protein determination was made using the bicichoninic acid protein assay (Thermo Fisher Scientific). A representation of samples from all experimental groups (including both the intact and lesion sides) was run on four different 96-well plates. In control animals, there was a slightly higher basal concentration of VEGF in the striatum compared with the substantia nigra pars reticulata (39.3 ± 2.2 and 27.8 ± 2.4 pg/g total protein, respectively); however, no significant treatment effects were seen on the intact sides of either structure. Therefore, to compensate for small variations in absolute values between plates, data from the lesioned side were expressed as a percentage of those from the intact side in each animal.

Astrocytic cultures and drug treatments

E18 timed-pregnant female Sprague-Dawley rats (Charles River) were anaesthetized with pentobarbital (65 mg/kg, Sigma) and embryos were removed. Striata and cortices were dissected in 1× Hank's buffered salt solution under a dissecting microscope, and dissociated in culture medium (50% Dulbecco's modified eagle medium, 50% Dulbecco's modified eagle medium F12, supplemented with 10% foetal bovine serum and penicillin/streptomycin, 100 U/ml each). Astrocytes were plated onto uncoated T-75 flasks. After 48 h, media was replaced with Dulbecco's modified eagle medium containing 10% foetal bovine serum and penicillin/streptomycin. After 4 weeks of maturation, cells were dissociated with Tryp-LE (Gibco-Invitrogen) and replated onto 6-well plates coated with polyethylenimine (1:500 diluted; Sigma) and foetal bovine serum, and grown for another 10 days before treatment. Drugs used for this experiment were: dopamine, a D1-class agonist (SKF-82958) and an antagonist (SCH23390), a D2-class agonist (Quinpirole) and an antagonist (Eticlopride) (all from Sigma). Drugs were applied for 3 h at a concentration of 50 μM (0.5% dimethylsulphoxide in controls). The incubation interval was chosen to mimic *in vivo* drug exposure and to allow time for messenger RNA regulation. Previous studies examining the effects of monoamines on growth factor response in astrocytes have indeed reported a peak in protein secretion at 6–24 h (Ohta *et al*., 2003; Mele *et al*., 2010).

Quantitative polymerase chain reaction of rat and human VEGF-A

RNA was extracted from rat astrocyte cultures using the Micro to Midi RNA extraction kit according to the manufacturer's protocol (Ambion). Human RNA was extracted with the RNAgents® kit (Promega Corporation) followed by a final cleaning step with RNeasy® columns (Qiagen). All samples were examined in an analytical gel and with the Bioanalyzer 2100 (Agilent). Human samples with RNA integrity

numbers >6 were included in the polymerase chain reaction assay. Complementary DNA was synthesized from 1 μg of total RNA with the iScript™ cDNA Synthesis kit (Bio-Rad). Primer sets for the VEGF gene were designed with the help of Primerblast (http://www.ncbi.nlm.nih.gov/tools/primer-blast) (Supplementary Table 1). Melt curve analysis and polyacrylamide gel electrophoresis were used to confirm the specificity of each primer pair. Quantitative polymerase chain reactions were carried out using a Stratagene ThermoCycler and Brilliant II SYBR® Green Supermix (Agilent Technologies). Polymerase chain reactions cycling conditions were as follows: an initial step of 95°C for 10 min, followed by 40 cycles of: 95°C for 15 s, 60°C for 15 s, 75°C for 15 s. Data were collected between 75°C and 80°C depending on amplicon melting temperature. Data were collected from standard curves and all samples were examined in duplicate. Two different VEGF-A primer pairs were used for the human study and three different VEGF-A primer pairs for the rat astrocytic cultures, which detect all known VEGF-A splice variants. Human VEGF-A data were normalized to the internal controls β-actin, integral membrane protein IIB and filamin A, and rat data were normalized to the internal controls β-actin, 18 s RNA, general transcription factor IIB and α-tubulin (Supplementary Table 1).

Statistical analysis

All data are presented as group means ± SEM. The abnormal involuntary movement scores per testing session during the chronic drug treatment periods were analysed using repeated measures ANOVA. This test provides valuable information on the interaction between a time factor (testing session) and a group category (treatment) that is not readily available in non-parametric tests. Relevant pairwise differences were analysed by *post hoc* Tukey's honestly significant difference test and confirmed by non-parametric Mann–Whitney U-test. All other data were analysed with one-factor ANOVA and *post hoc* Student–Newman–Keul's test. Statistical significance α was set at 0.05. Precise *P*-values from the ANOVAs are reported, whereas *post hoc* comparisons are reported as being significant or non-significant. Statistical analyses were performed with SPSS version 17.0 (SPSS).

Results

Dose-dependent effect of L-dopa treatment on angiogenesis markers and blood–brain barrier leakage

Previous studies have indicated that angiogenic activity and blood–brain barrier leakage may accompany the neurodegeneration of the nigrostriatal pathway (Barcia *et al*., 2005; Carvey *et al*., 2005; Kortekaas *et al*., 2005; Bartels *et al*, 2008). To obtain conclusive evidence that, in our animal model of LID, the extent of angiogenesis and blood–brain barrier involvement is dictated by the dopaminergic treatment (as opposed to the pre-existing lesion), we searched for a possible dose-dependent effect of L-dopa on immunohistochemical indices of angiogenesis and increased blood–brain barrier permeability, namely, the number of bromodeoxyuridine/laminin double-labelled cells, nestin and endothelial barrier antigen immunoreactivity on blood vessels and albumin immunoreactivity in the brain parenchyma. These markers are significantly altered in the lateral striatum, the globus pallidus, the entopeduncular nucleus and the substantia nigra pars reticulata in L-dopa-treated dyskinetic animals (Westin *et al*., 2006; Lindgren *et al*., 2009). A similar pattern of alterations was found in the present study, although quantitative analyses were limited to the lateral striatum (Fig. 2A–H) and the substantia nigra pars reticulata (Fig. 2I–P).

The two treatment regimens compared in this experiment consisted of 6 mg/kg ($n = 6$) or 25 mg/kg L-dopa ($n = 6$), administered as twice daily injections for 21 days (as in Lindgren *et al*., 2007; Picconi *et al*., 2008). As expected, the higher dose of L-dopa resulted in an earlier and more severe development of abnormal involuntary movements [Fig. 3A; $F(2,16) = 53.05$, $P_{treatment} < 0.0001$, $P_{time} < 0.0001$ and $P_{interaction} < 0.0001$]. All animals treated with the higher dose of L-dopa developed dyskinesia, while two out of six animals treated with the lower dose remained non-dyskinetic.

To obtain indices of angiogenesis, we counted the number of bromodeoxyuridine-positive cells co-localized with laminin-immunoreactivity (bromodeoxyuridine was administered only during the last 3 days of L-dopa treatment) and we measured the amount of nestin immunostaining associated with microvessel profiles. Saline-treated 6-hydroxydopamine lesioned controls did not display any evident upregulation of these markers on the side ipsilateral to the lesion compared with the intact side. In contrast, L-dopa-treated rats showed an enhanced expression. In the striatum, the number of bromodeoxyuridine/laminin-positive cells did not differ significantly between the two L-dopa dose groups, both being significantly different from saline controls [Fig. 3B; $F(2,16) = 4.89$, $P = 0.026$]. In the substantia nigra pars reticulata, the number of bromodeoxyuridine/laminin cells was 30% larger in the high-dose L-dopa group compared with the low-dose animals [Fig. 3B, right; $F(2,16) = 28.66$, $P < 0.0001$; Fig. 2I–J]. Levels of microvascular nestin immunostaining were 2-fold larger in the high-dose L-dopa group versus the low-dose group in both the striatum and the substantia nigra pars reticulata [Fig. 3C; $F(2,16) = 13.26$, $P_{striatum} = 0.001$; $F(2,16) = 25.04$, $P_{substantia\ nigra\ pars\ reticulata} < 0.0001$; Fig. 2C, D and K–L].

As indices of increased blood–brain barrier permeability, we examined the extent of endothelial barrier antigen downregulation and parenchymal albumin immunoreactivity. In the striatum, only the high-dose L-dopa group showed a significant reduction in endothelial barrier antigen immunostaining relative to control levels [Fig. 3D; $F(2,16) = 4.31$, $P = 0.001$]. In the substantia nigra pars reticulata, the reduction was significant in both treatment groups, although it was more pronounced following high-dose L-dopa treatment [Fig. 3D $F(2,16) = 19.62$, $P < 0.0001$; $P < 0.05$ for high versus low dose group; Fig. 2M and N]. Parenchymal albumin immunoreactivity, an index of blood–brain barrier hyperpermeability, also showed clear dose-dependent changes [Fig. 3E; $F(2,16) = 13.16$, $P_{striatum} = 0.001$; $F(2,16) = 20.39$, $P_{substantia\ nigra\ pars} < 0.0001$], which were particularly evident in the substantia nigra pars reticulata ($P < 0.05$ for high- versus low-dose group; Fig. 2O and P). These results indicate that larger doses of L-dopa induce higher angiogenic activity and more blood–brain barrier involvement compared with lower doses. These dose-dependent effects were more distinct in the

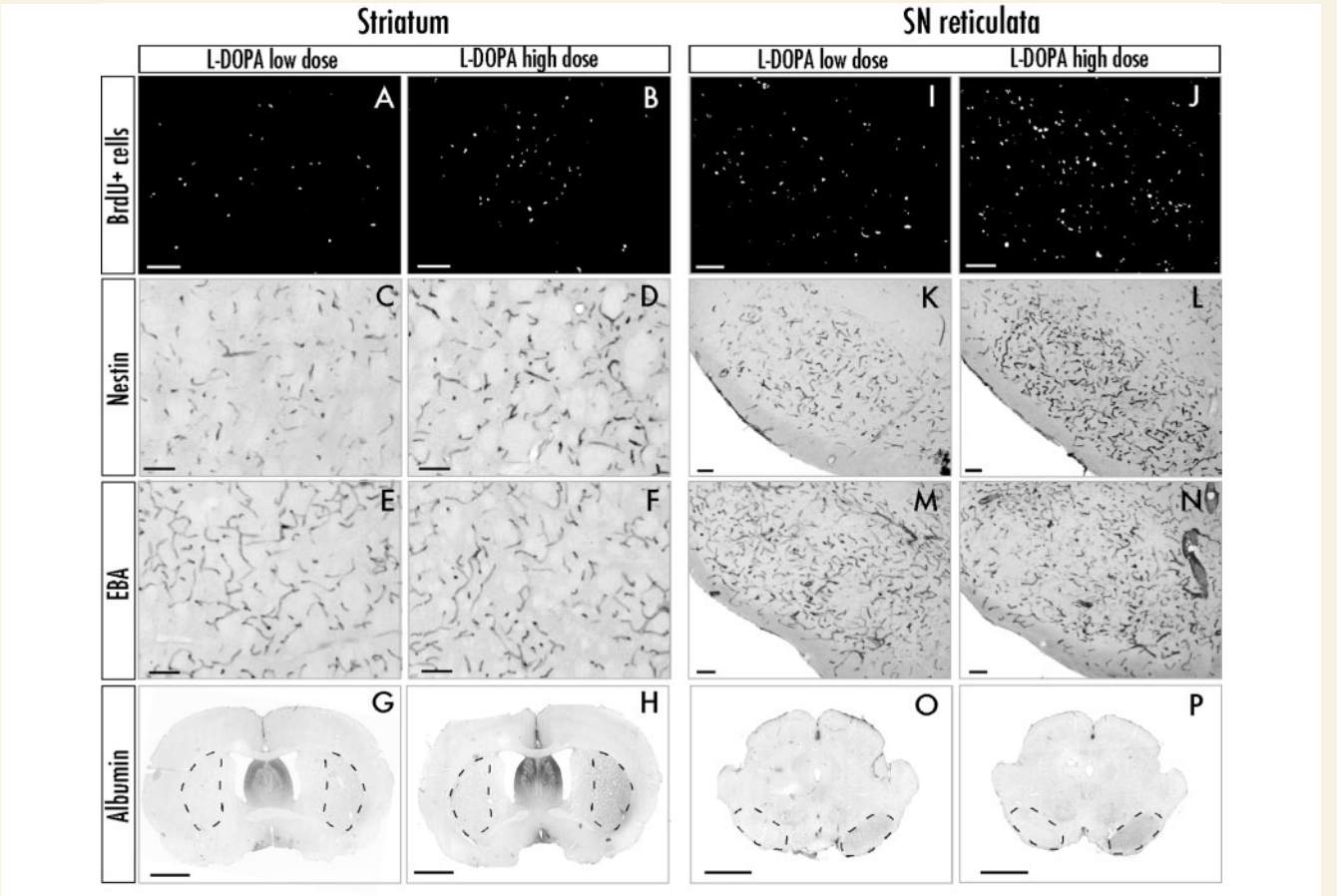

Figure 2 Representative photomicrographs show the expression of angiogenesis markers in the striatum and substantia nigra pars reticulata (SNr). Only cases treated with low dose and high-dose L-dopa are shown (saline animals do not show significant alterations of these markers on either side of the brain); (Westin *et al*., 2006, Lindgren *et al*., 2009). (**A**, **B**, **I** and **J**) Epifluorescence photomicrographs of bromodeoxyuridine (BrdU)-positive cells. (**C**, **D**, **K** and **L**) Bright-field photomicrographs of nestin immunopositive vessels. (**E**, **F**, **M** and **N**) Endothelial barrier antigen (EBA) (its loss indicates blood–brain barrier malfunction). (**G**, **H**, **O** and **P**) Overview pictures of striatal and midbrain sections used to measure albumin optical density in the lateral caudate–putamen and the substantia nigra pars reticulata. Regions of interest are encircled by dashed lines. Scale bars = 100 μm (**A–F** and **I–N**), 2 mm (**G**, **H**, **O** and **P**).

basal ganglia output structure substantia nigra pars reticulata, which has a stronger angiogenic response to the treatment (Westin *et al*., 2006; Lindgren *et al*., 2009).

Dose-dependent induction of vascular endothelial growth factor by chronic L-dopa treatment

An additional set of rats received similar treatments (L-dopa low dose; 6 mg/kg, high dose; 25 mg/kg) and were prepared for an analysis of VEGF protein expression using both enzyme-linked immunosorbent assay and immunohistochemistry. Quantification of VEGF protein levels by enzyme-linked immunosorbent assay showed a significantly increased expression following L-dopa treatment in both the striatum and the substantia nigra pars reticulata on the side ipsilateral to the lesion [Fig. 4A; $F(2,21) = 9.59$, $P_{striatum} = 0.001$; $F(2,21) = 16.25$, $P_{substantia\ nigra\ pars\ reticulata} < 0.0001$]. In the striatum, VEGF protein levels were elevated by ~25 and ~45% above control values in the low- and high-dose L-dopa group, respectively, but the difference between the two groups did not reach significance. In the substantia nigra pars reticulata, on the other hand, there was a clear dose-dependent effect, and the magnitude of VEGF upregulation was markedly larger following high-dose (214%) compared with low-dose L-dopa treatment (58% increase above control values) (Fig. 4A). Upregulation of VEGF by chronic L-dopa treatment was confirmed at the messenger RNA level through an analysis of gene chip microarray data produced in a previously published study (Konradi *et al*., 2004), and verified using *in situ* hybridization histochemistry (Supplementary Table 2 and Supplementary Fig. 2).

To examine the cellular pattern of VEGF protein expression, immunostaining was performed on sections through the structures of interest. In the dopamine-denervated hemisphere, VEGF

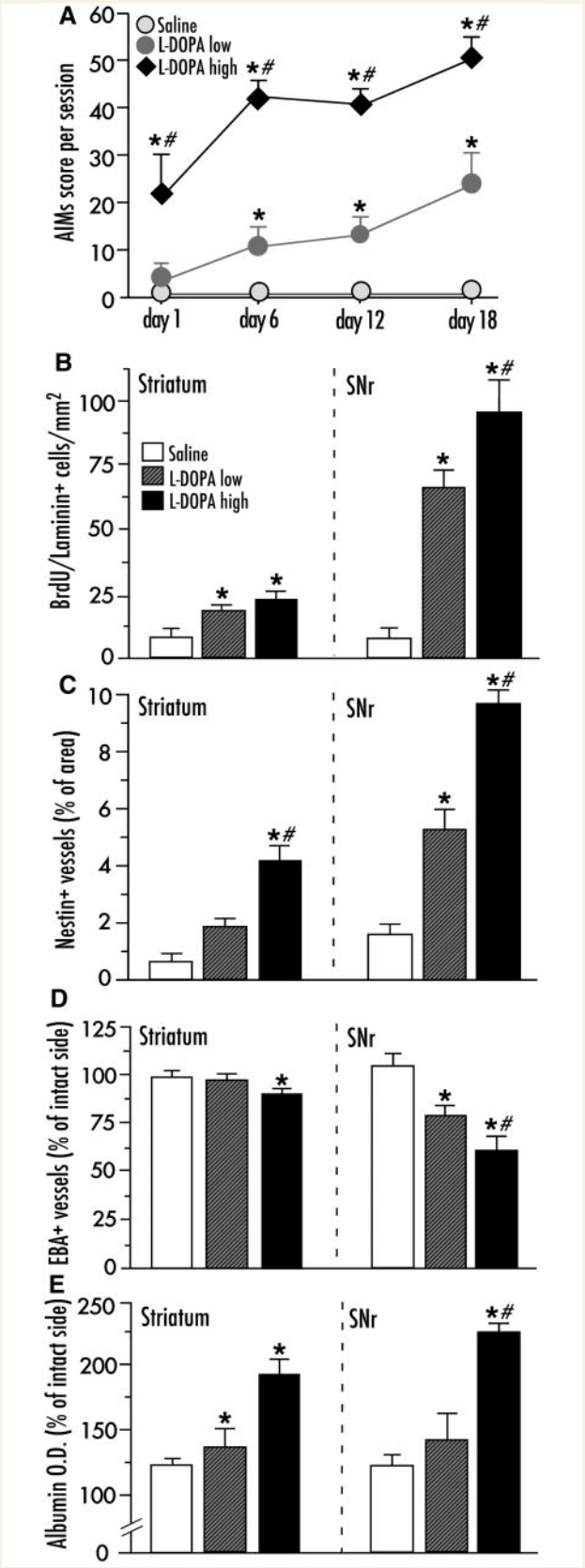

Figure 3 The development of dyskinesia and the associated angiogenic activity are dose-dependently induced by chronic L-dopa treatment. (**A**) Development of dyskinesia during 21 days of treatment, high-dose L-dopa (25 mg/kg, $n = 6$), low-dose L-dopa (6 mg/kg, $n = 6$), saline-treated controls ($n = 6$). Abnormal involuntary movement scores are expressed as the sum of limb, axial and orolingual scores per session. Repeated measures ANOVA followed by Tukey's Honestly Significant Difference *post hoc* comparison. (**B–E**) Indices of angiogenesis and increased blood–brain barrier permeability in the striatum and substantia nigra pars reticulata (SNr) are dose-dependently regulated by L-dopa treatment. (*Left*) Data from the striatum; (*right*) data from the substantia nigra pars reticulata, from the same animals as in (**A**). (**B**) Endothelial proliferation (counts of bromodeoxyuridine-labelled cells on laminin-positive blood vessel profiles); (**C**) upregulation of nestin on blood vessel profiles; (**D**) Downregulation of endothelial barrier antigen (EBA) in blood vessels, and (**E**) parenchymal albumin extravasation. One-factor ANOVA followed by *post hoc* Student–Newman–Keul's, $P < 0.05$; *versus saline, #versus L-dopa low-dose group. All values are expressed as mean ± SEM.

immunoreactivity was clearly stronger in L-dopa-treated rats compared with saline-treated controls (Fig. 4B). On bright-field microscopy, VEGF immunoreactivity showed a punctate pattern that was widely distributed in the brain parenchyma but particularly dense along the walls of blood vessels and in astrocytic-like structures (Fig. 4B). A definite proof of astrocytic localization was achieved using dual- and triple antigen immunofluorescence followed by confocal microscopy, which revealed VEGF expression in GFAP-positive astrocytic processes located in close proximity to the blood vessels (Fig. 4C). Moreover, virtually all VEGF-immunoreactive cell bodies stained positively for GFAP (Supplementary Fig. 3A and B). In contrast, we did not observe any co-localization of VEGF with established markers of resting or activated microglial cells (CD11b/OX42 and CD68/ED-1, respectively; Supplementary Fig. 3C and D).

In an attempt to verify whether astrocytes can be directly stimulated to produce VEGF by an increased dopamine tone, we used rat primary astrocytes from both striatum and cortex, which were incubated with a fixed concentration (50 μM) of dopaminergic agents prior to measuring VEGF-A messenger RNA levels by quantitative polymerase chain reaction ($n = 6$ per condition). In a first experiment, cells were treated with dopamine only, which induced a significant upregulation VEGF-A messenger RNA expression in both striatal and cortical astrocytes [Fig. 5A; $F(5,35) = 58.24$, $P_{striatal} < 0.0001$; $F(5,35) = 58.24$, $P_{cortical} < 0.0001$]. In a second experiment, astrocytes were incubated with agonists or antagonists of D1- or D2-class receptors. The direct D1 agonist SKF-82958 induced a large upregulation of VEGF-A messenger RNA (14-fold of control values in striatal cultures), while the D1 antagonist SCH23390 had no effect. The D2 agonist, quinpirole did not produce any significant change in VEGF-A messenger RNA levels, while the D2 antagonist eticlopride induced a 6-fold increase compared with controls, differing significantly from all the other conditions [Fig. 5B; $F(5,35) = 60.95$, $P_{striatal} < 0.0001$; $F(5,35) = 48.25$, $P_{cortical} < 0.0001$].

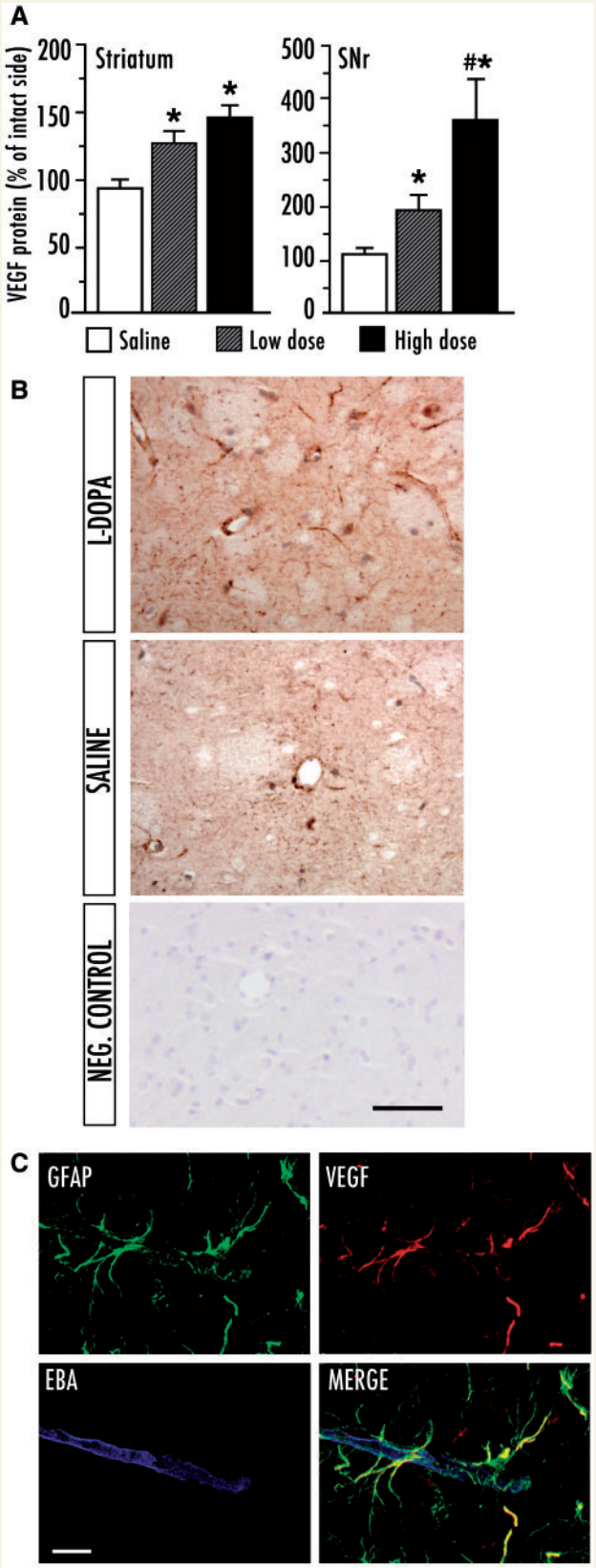

Figure 4 Levels of vascular endothelial growth factor (VEGF) are dose-dependently upregulated in the basal ganglia following chronic L-dopa treatment. (**A**) VEGF protein levels (measured with enzyme-linked immunosorbent assay) in the striatum and substantia nigra pars reticulata (SNr). L-Dopa high dose ($n = 6$), L-dopa low dose ($n = 6$), saline ($n = 10$). Results from the L-dopa-denervated hemisphere are expressed as a percentage of the intact side in each subject to normalize for inter-assay variability. One-factor ANOVA followed by *post hoc* Student–Newman–Keul's; $P < 0.05$ *versus saline, #versus low dose. (**B**) Bright-field VEGF immunohistochemistry on striatal sections from L-dopa and saline-treated rats. The negative control was obtained by pre-absorbing the primary antiserum with a 5-fold larger concentration of the immunizing peptide (the section was lightly counterstained with Mayer's haematoxylin to visualize the tissue). (**C**) Laser scanning confocal microscopy of triple immunofluorescence for glial fibrillary astrocytic protein (GFAP), VEGF and endothelial barrier antigen (EBA). Endothelial barrier antigen was used as an endothelial marker, and areas of reduced immunopositivity could be seen in proximity of the VEGF-positive astrocytes. Scale bar = 50 μm (**B**) and 10 μm (**C**).

Antidyskinetic and anti-angiogenic effects of VEGF receptor 2 tyrosine kinase antagonism

The small molecule inhibitor of VEGFR2 tyrosine kinase vandetanib (Wedge *et al.*, 2002) was administered in combination with an escalating dose regimen of L-dopa during a 3-week treatment period. A low dose of L-dopa (6 mg/kg/day) induced similar abnormal involuntary movement scores in vandetanib- and vehicle-treated animals (Fig. 6A). Upon administration of 12 mg/kg/day L-dopa, there was a significant interaction between treatment and time [Fig. 6B; $F(1,8) = 4.49$, $P < 0.0001$], but the difference between vandetanib and vehicle did not reach significance on the *post hoc* comparisons (Fig. 6B). When the L-dopa dose was further increased to 24 mg/kg/day, the difference between vandetanib and vehicle groups became pronounced [Fig. 6C; repeated measures ANOVA; $F(1,20)$ $P_{treatment} < 0.0128$, $P_{time} < 0.0001$ and $P_{interaction} < 0.0001$, $P < 0.05$ for vandetanib versus vehicle at 20–120 min post L-dopa injection]. Dyskinesia scores per monitoring period were lower in vandetanib-treated animals during the beginning, the peak and the plateau phase of the abnormal involuntary movements curve (20–140 min), but not in its declining phase (160–240 min; Fig. 6C). The sum of abnormal involuntary movement scores per testing session during the peak and plateau phase differed significantly between the groups (Fig. 6D; repeated measures ANOVA, $P_{treatment} < 0.0001$, $P_{time} < 0.0001$ and $P_{interaction} < 0.0001$), being significantly lower in vandetanib versus vehicle treatment on the last two testing sessions (Days 20 and 22; Fig. 6D).

The cylinder test of forelimb akinesia did not show any negative effect of vandetanib treatment on the rats' motor performance either OFF L-dopa [Fig. 6E, $F(3,30) = 0.51$, $P = 0.68$] or ON L-dopa (Fig. 6F). Following the administration of L-dopa, a similar reversal of forelimb use asymmetry occurred in vandetanib- and vehicle-treated animals [Fig. 6F; $F(3,30) = 13.88$, $P < 0.0001$]. The total number of wall contacts in the cylinder (representing a measure of overall motor activity) was not affected by vandetanib either [Fig. 6G, $F(3,30) = 0.32$, $P = 0.81$].

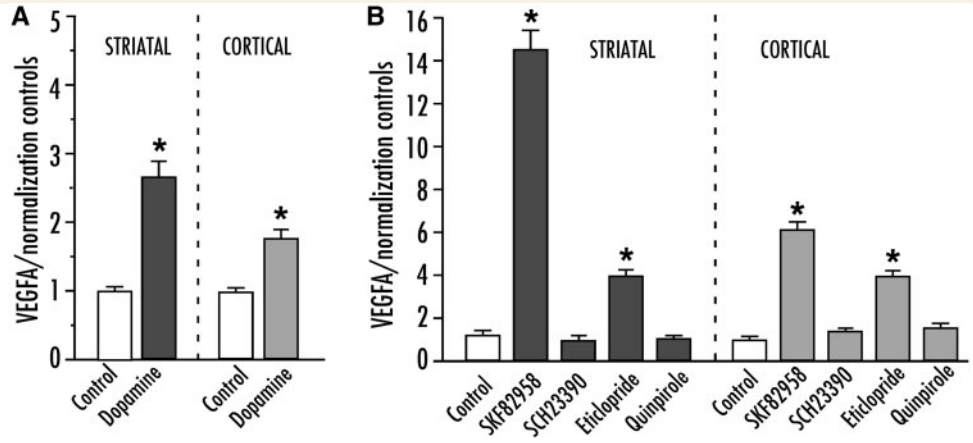

Figure 5 VEGF messenger RNA is upregulated following dopaminergic stimulation in primary cerebral astrocytes. (**A**) Quantitative polymerase chain reaction from striatal (*left*) or cortical (*right*) astrocytes incubated with 50 μM of dopamine or control (DMSO) for 3 h. (**B**) VEGF messenger RNA levels following stimulation with a direct D1 agonist (SKF82958), a D1 antagonist (SCH23390), a D2 agonist (quinpirole), and a D2 antagonist (eticlopride) applied for 3 h ($P < 0.0001$ for all statistical comparisons in **A** and **B**). One-factor ANOVA followed by *post hoc* Student–Newman–Keul's; $P < 0.05$ *versus all other groups. Values are expressed as mean ± SEM.

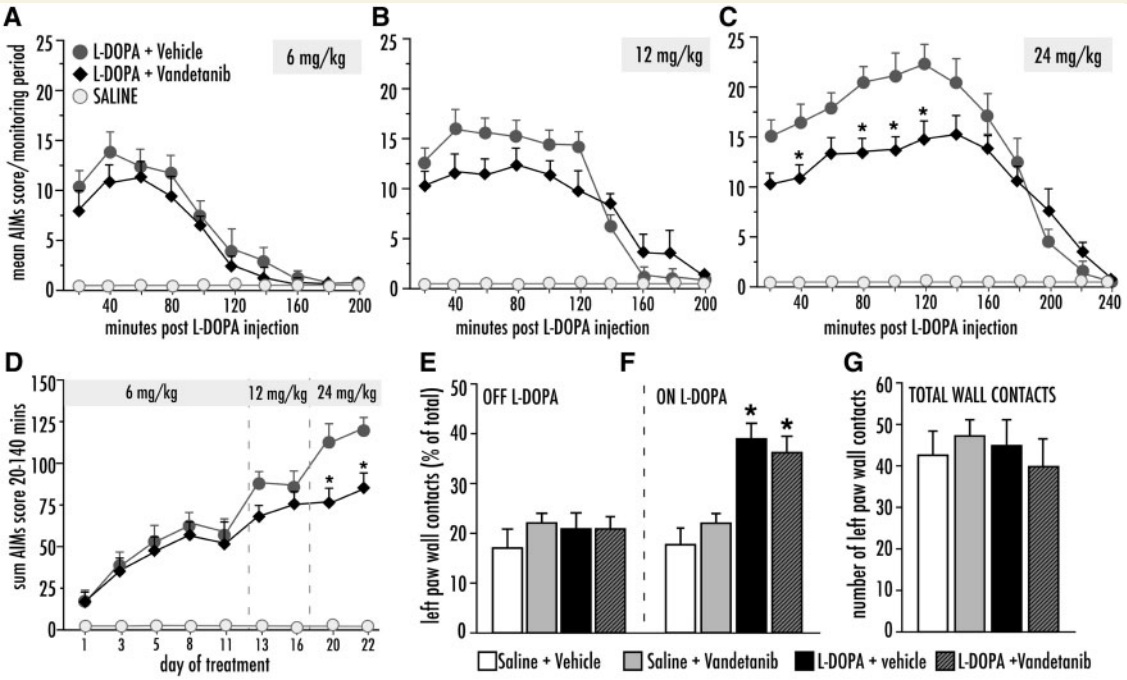

Figure 6 Co-treatment with Vandetanib attenuated the development of abnormal involuntary movements (AIMs) upon chronic treatment with L-DOPA. Rats were treated with L-DOPA at increasing doses (day 1–12, 6 mg/kg; day 13–19, 12 mg/kg; day 20–22, 24 mg/kg). (**A**) Development of AIMs following one L-DOPA injection at the low-dose treatment (6 mg/kg), (**B**) medium dose treatment (12 mg/kg), and (**C**) high dose treatment (24 mg/kg). L-DOPA + vehicle ($n = 12$), L-DOPA + Vandetanib ($n = 10$), saline ($n = 12$). (**D**) Global AIMs scores after each dose and test. Repeated measures ANOVA (in **C** and **D**), followed by Tukey's HSD *post hoc* comparisons where appropriate. $P < 0.05$, *versus L-DOPA + vehicle. (**E–G**) Cylinder test of forelimb use asymmetry showed no difference between the groups treated with Vandetanib or vehicle treated groups. (**E**) Performance measured 'OFF' L-DOPA (day 12) or (**F**) Performance 'ON' L-DOPA (90 minutes post L-DOPA injection), (**G**) total activity (total touches against cylinder wall). One-factor ANOVA followed by *post hoc* Student-Newman Keul's. Values expressed as mean S.E.M. *$P < 0.05$ versus saline-treated groups.

Upon immunohistochemical examination, a significant inhibition of L-dopa-induced angiogenesis was found in animals that received vandetanib co-treatment (Fig. 7A–D). L-dopa-induced endothelial proliferation (number of bromodeoxyuridine/laminin cells) was efficiently blocked by vandetanib in the striatum [$F(2,30) = 20.37$, $P < 0.0001$], while it was significantly reduced, although not completely inhibited, in the substantia nigra pars reticulata [Fig. 7A; $F(2,30) = 43.99$ $P < 0.0001$]. Nestin

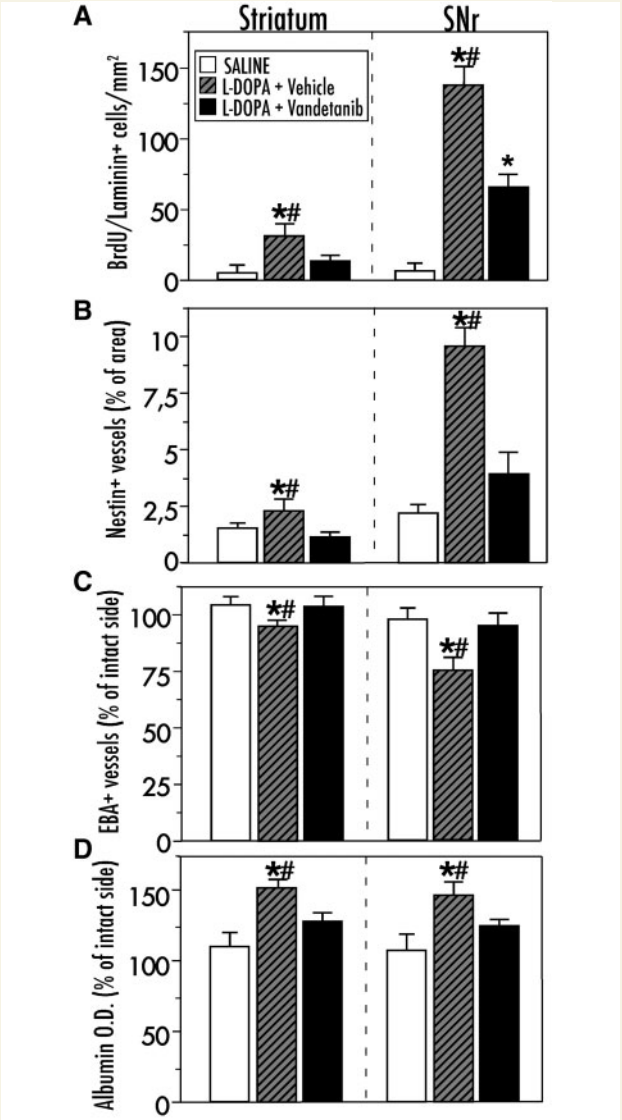

Figure 7 Vandetanib co-treatment blocked L-dopa-induced angiogenic activity in the basal ganglia. Endothelial proliferation ($BrdU^+$/$Laminin^+$ cells) (**A**), nestin upregulation (**B**), downregulation of endothelial barrier antigen (EBA; **C**), and parenchymal albumin extravasation (**D**). L-dopa + vehicle ($n = 12$), L-dopa + vandetanib ($n = 10$), saline ($n = 12$). One-factor ANOVA followed by *post hoc* Student–Newman–Keul's. $P < 0.05$ *versus saline controls, #versus L-dopa + vandetanib.

upregulation was blocked by vandetanib in both the striatum and the substantia nigra pars reticulata [Fig. 7B; $F(2,30) = 7.92$, $P_{striatum} = 0.002$, $F(2,30) = 7.38$, $P_{substantia\ nigra\ pars\ reticulata} = 0.003$]. Indices of blood–brain barrier permeability were normalized by vandetanib, which completely prevented both the downregulation of endothelial barrier antigen [Fig. 7C; $F(2,30) = 4.40$, $P_{striatum} = 0.021$; $F(2,30) = 16.80$, $P_{substantia\ nigra\ pars\ reticulata} < 0.0001$] and the parenchymal accumulation of albumin [Fig. 6D; $F(2,30) = 5.75$, $P_{striatum} = 0.003$; $F(2,30) = 11.58$, $P_{substantia\ nigra\ pars\ reticulata} < 0.0001$].

Indices of angiogenesis are upregulated in the basal ganglia of dyskinetic patients with Parkinson's disease

Immunohistochemical indices of angiogenesis were examined in sections through the posterior basal ganglia from dyskinetic patients with Parkinson's disease ($n = 12$), patients with Parkinson's disease lacking clinical records of LID ($n = 9$) and neurologically healthy controls ($n = 6$). Demographic and clinical data from this set of cases are shown in Table 1. Total microvessel density was estimated by quantitative image analysis of the pan-endothelial marker CD34 (Kalaria *et al.*, 1992), which was expressed exclusively on vessel-like structures (Fig. 8A). In the putamen, the levels of CD34 immunoreactivity were 2-fold larger in dyskinetic Parkinson's disease subjects relative to non-dyskinetic cases and controls [Fig. 8C; $F(2,23) = 6.71$, $P = 0.005$; $P < 0.05$ for dyskinetic Parkinson's disease versus each of the other groups]. The external globus pallidus and internal globus pallidus exhibited an overall lower microvessel density compared with the putamen in all cases, although a significant increase in CD34 immunoreactivity could be detected in the dyskinetic Parkinson's disease group also in these structures [external globus pallidus, Fig. 8F, $F(2,23) = 5.84$, $P = 0.008$; internal globus pallidus, Fig. 8I; $F(2,23) = 7.80$, $P = 0.002$].

Nestin immunopositivity was seen exclusively on the inner lining of blood vessels and was sparsely distributed in control cases, consistent with the low rate of endothelial turnover that is normally found in the adult brain (Mokry *et al.*, 1999, 2004) (Fig. 9). In the putamen, the levels of nestin immunoreactivity were over 10-fold larger in dyskinetic Parkinson's disease cases when compared with controls [Fig. 9C; $F(2,23) = 6.54$, $P = 0.005$; $P < 0.05$ for dyskinetic Parkinson's disease versus each of the other two groups] and showed an inverse correlation with the time to onset of dyskinesia (correlation coefficient = −0.66, $P = 0.048$). Putaminal nestin levels tended to be elevated also in the non-dyskinetic cases with Parkinson's disease that, however, did not differ significantly from the control group. The dyskinetic Parkinson's disease brains showed increased nestin expression also in the external globus pallidus [Fig. 9F; $F(2,23) = 6.56$, $P = 0.005$; 175% increase versus both controls and non-dyskinetic Parkinson's disease, $P < 0.05$], and in the internal globus pallidus [Fig. 9I; $F(2,23) = 3.56$, $P = 0.045$], although pairwise group comparisons did not reach statistical significance in the latter structure.

Additional sections from the same set of patients were immunostained for VEGF and albumin. These markers were difficult to quantify due to their widespread but uneven expression, and a large variability between subjects. However, we noticed that cases with the highest expression of CD34 and nestin also had the highest immunoreactivity for VEGF and albumin. Figure 10 shows two representative cases with Parkinson's disease that consistently exhibited high versus low expression of the four markers under investigation ('high angiogenic index', Fig. 10A–G; 'low angiogenic index' Fig. 10B–H). In the cases with high angiogenic activity, the pattern of VEGF expression was similar to that found in L-dopa-treated dyskinetic rats, consisting of punctate immunoreactivity particularly enriched in the proximity of blood vessels

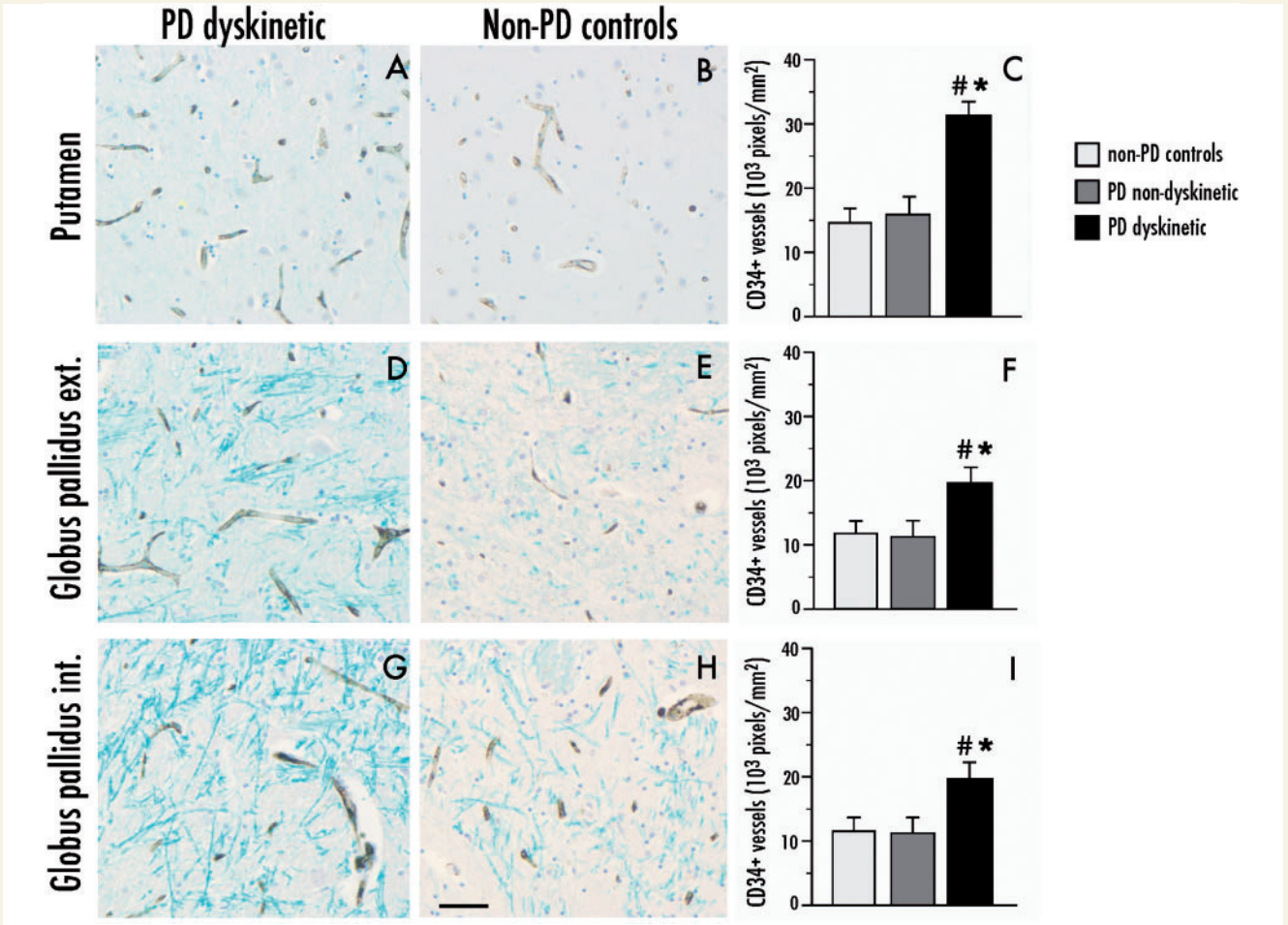

Figure 8 Parkinson's Disease (PD) dyskinetic patients have an increased number of CD34-immunostained blood vessel profiles in the basal ganglia. Representative photomicrographs of CD34 expression in dyskinetic and non-dyskinetic patients in the putamen (**A** and **B**), external (ext.) and internal (int) globus pallidus in (**D** and **E**) and (**G** and **H**), respectively. Bar graphs to the right show the number of CD34-immunopositive pixels per sampling frame in the putamen (**C**), external and internal globus pallidus (**F** and **I**, respectively) from dyskinetic patients with Parkinson's disease (PD dyskinetic, $n = 11$), non-dyskinetic patients with Parkinson's disease (PD non-dyskinetic, $n = 9$) and neurologically healthy controls (non-PD controls, $n = 6$). One-factor ANOVA followed by *post hoc* Student–Newman–Keul's, $P < 0.05$, *versus non-Parkinson's disease controls, #versus non-dyskinetic Parkinson's disease. Scale bar = 50 μm.

(Fig. 10E, arrowhead). Sparse VEGF-immunoreactive cell bodies also occurred. Albumin immunoreactivity was heterogeneously distributed, but areas with the highest parenchymal staining consistently displayed albumin-positive cell bodies (Fig. 10G), which is in line with the occurrence of albumin-immunoreactive astrocytes under conditions of blood–brain barrier leakage (Rigau *et al.*, 2007).

Putaminal upregulation of VEGF messenger RNA in dyskinetic patients

Putamen tissue samples from an independent set of dyskinetic and non-dyskinetic patients with Parkinson's disease and matched controls were used for quantitative analysis of VEGF-A messenger RNA by quantitative polymerase chain reaction. All data from this set of cases are shown in Table 2. In the dyskinetic Parkinson's disease group ($n = 11$), VEGF-A messenger RNA levels were significantly upregulated (increase by 48% over normalization controls) compared with both the non-dyskinetic Parkinson's disease cases ($n = 12$) and the control subjects [$n = 18$; $F(2,38) = 4.881$, $P = 0.013$; Table 2).

Discussion

This study demonstrates that VEGF is involved in the pathophysiology of LID in an animal model of Parkinson's disease. Dose-dependent patterns of VEGF upregulation and angiogenic activity were produced by L-dopa in the striatum and the substantia nigra pars reticulata, two structures that mediate the motor effects of dopamine replacement therapy (Robertson and Robertson, 1989). VEGF expression was mainly localized to astrocytes and astrocytic processes apposed to blood vessels (astrocytic end-feet). Moreover, rat primary astrocytic cultures reacted highly to exogenous dopaminergic stimulation with an

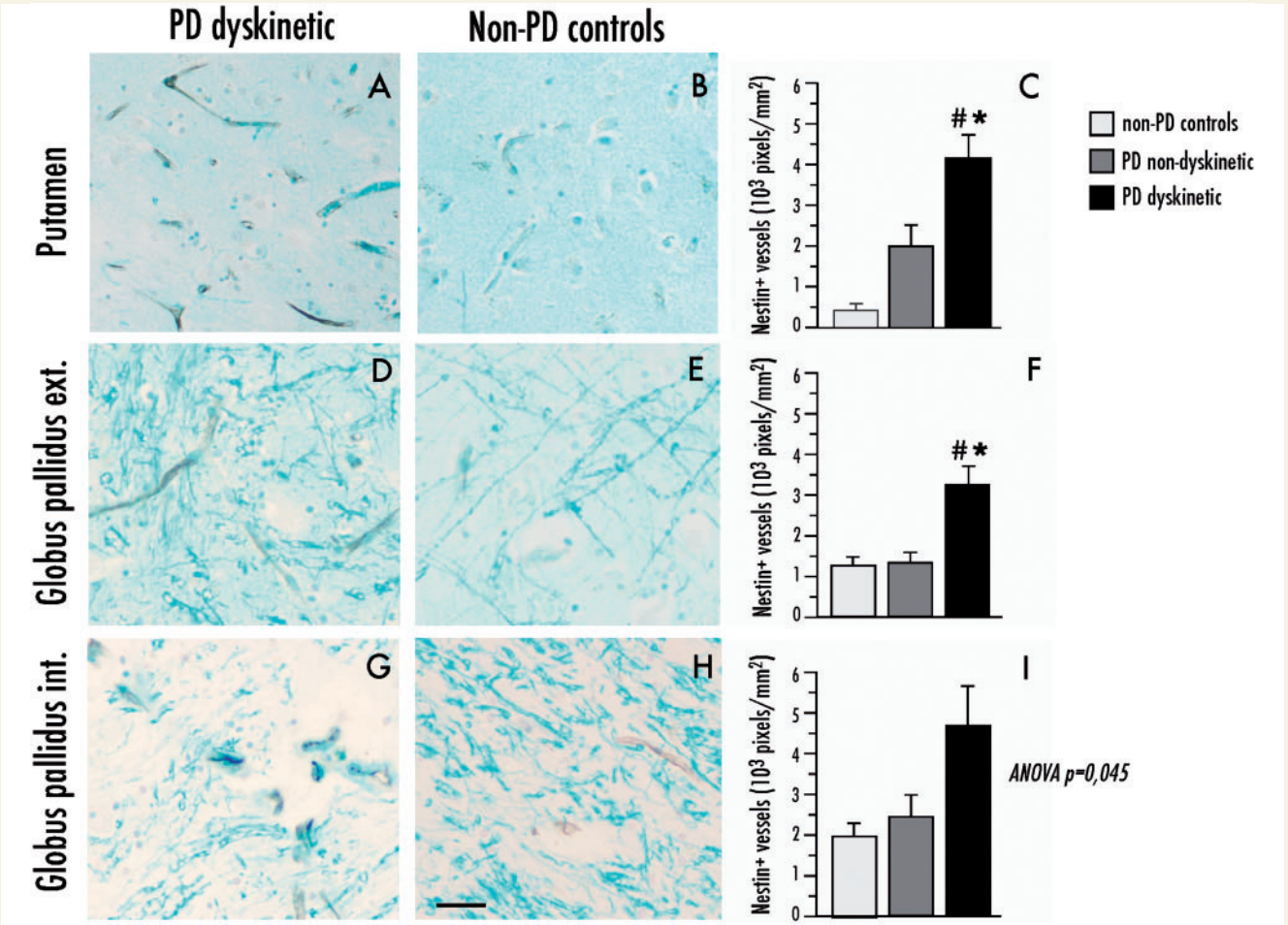

Figure 9 Parkinson's disease (PD) dyskinetic patients have an increased expression of the immature endothelial marker, nestin on blood vessels in the basal ganglia. Representative photomicrographs of nestin expression in dyskinetic and non-dyskinetic patients in the putamen (**A** and **B**), external (ext.) and internal (int.) globus pallidus in (**D** and **E**) and (**G** and **H**), respectively). Bar graphs to the *right* show quantification of nestin immunopositive pixels in the putamen (**C**), external and internal globus pallidus (**F** and **I**, respectively) from dyskinetic patients with Parkinson's disease (PD dyskinetic, $n = 11$), non-dyskinetic patients with Parkinson's disease (PD non-dyskinetic, $n = 9$) and neurologically healthy controls (non-PD controls, $n = 6$). One-factor ANOVA followed by *post hoc* Student–Newman–Keul's, $P < 0.05$, *versus non-Parkinson's disease controls, #versus non-dyskinetic Parkinson's disease. Scale bar = 25 μm.

upregulation of VEGF messenger RNA. The concomitant attenuation of L-dopa-induced abnormal involuntary movements and angiogenic activity by the high-affinity inhibitor of VEGFR2 signalling, vandetanib, indicates that VEGF contributes to the development of dyskinesia in this experimental model of Parkinson's disease. Congruent with the results from the rat model, post-mortem tissue from dyskinetic patients with Parkinson's disease showed enhanced microvascular density along with indices of active angiogenesis and elevated VEGF immunoreactivity. Putaminal upregulation of VEGF messenger RNA was found in an independent cohort of dyskinetic patients with Parkinson's disease. Taken together, our results indicate that VEGF is linked to the angiogenic activity that occurs in the parkinsonian brain during L-dopa treatment. Moreover, the findings corroborate previous suggestions that microvascular remodelling is an integral part of the maladaptive plasticity associated with LID.

Research regarding the involvement of the microvasculature in neurological disease is attracting growing interest. Altered neurovascular coupling and increased blood–brain barrier permeability are known to occur in several neurodegenerative and ischaemic disorders (Iadecola *et al*., 2004; Zlokovic *et al*., 2008; Attwell *et al*., 2010), although these changes have not been adequately addressed in Parkinson's disease. Post-mortem investigations on Parkinson's disease brains have reported microvascular pathology in the cerebral cortex (Farkas *et al*., 2000), an increased number of endothelial cells (Faucheux *et al*., 1999), and immunohistochemical evidence of VEGF upregulation in the substantia nigra pars compacta, with a variable degree of upregulation in the striatum (Wada *et al*., 2006). Also, two recent *in vivo* imaging studies have reported blood–brain barrier dysfunction in the midbrain of patients with Parkinson's disease (Kortekaas *et al*., 2005; Bartels *et al*., 2008). However, the medication history and therapeutic response to L-dopa were not considered in these investigations.

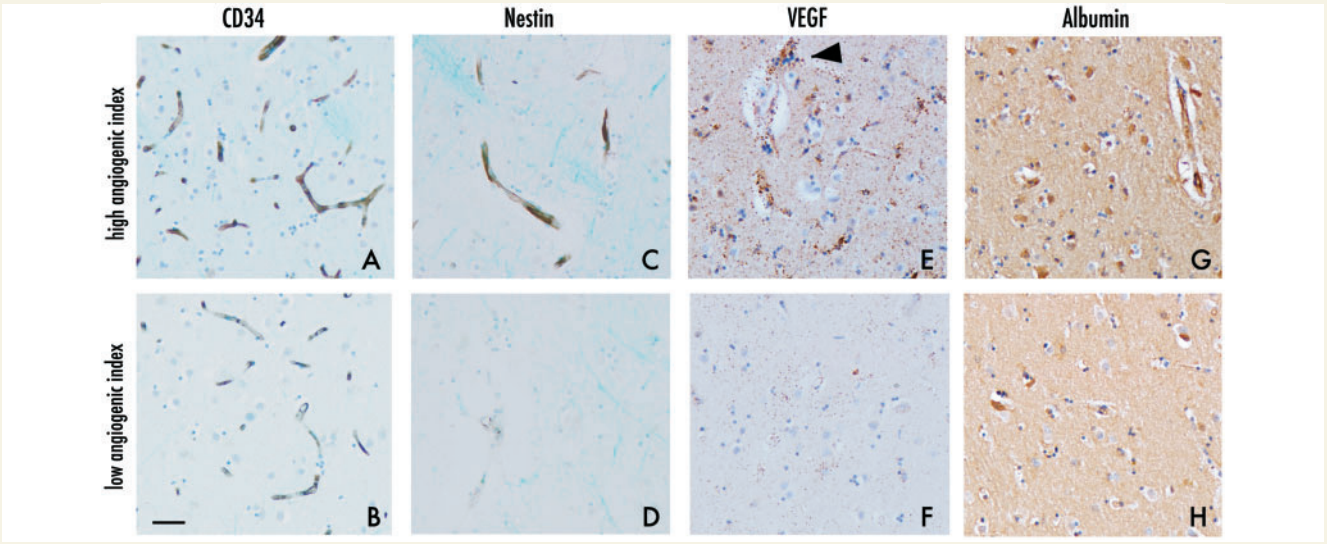

Figure 10 Patients with a high number of CD34- and nestin immunopositive blood vessels also show an increased expression of VEGF and albumin positive cells in the basal ganglia (*top*, 'high angiogenic index'). Representative bright-field photomicrographs in the putamen from cases with a 'high angiogenic index' (**A**, **C**, **E** and **G**) or a 'low angiogenic index' (**B**, **D**, **F** and **H**) show the expression of all markers under investigation: CD34 (**A** and **B**), nestin (**C** and **D**), VEGF (**E** and **F**), and albumin (**G** and **H**). Arrowhead in (**E**) shows punctate expression of VEGF at the border of a blood vessel. Scale bar = 25 μm.

Our study is the first to compare dyskinetic and non-dyskinetic Parkinson's disease cases on multiple indices of angiogenesis and VEGF upregulation. Some of the markers under investigation had not previously been examined in Parkinson's disease. One of these is nestin, an intermediate filament protein that is expressed by endothelial cells under conditions of active angiogenesis (Mokrý *et al*., 1999, 2004; Chmelova *et al*., 2010). While nestin was expressed at very low levels in control brains, a large number of blood vessels reacted positively for nestin in the dyskinetic Parkinson's disease cases. Moreover, putaminal levels of nestin immunostaining were inversely correlated with the time-to-onset of LID, indicating that the angiogenic activity was most pronounced in subjects developing dyskinesia earliest during their Parkinson's disease treatment. The overall microvascular density, estimated using the pan-endothelial marker CD34, also was significantly elevated in dyskinetic subjects relative to non-dyskinetic Parkinson's disease cases and controls. VEGF upregulation was seen in two sets of post-mortem cases using different techniques, of which only quantitative polymerase chain reaction analysis of VEGF messenger RNA was deemed suitable for statistical comparisons. Taken together, these results provide strong evidence of angiogenesis in the basal ganglia in advanced Parkinson's disease with dyskinesia.

Although cause–effects relationships cannot be inferred from post-mortem investigations, our studies in the rat provide important mechanistic clues. First, our results show that both VEGF induction and the expression of angiogenesis markers in the basal ganglia are sensitive to the extent of L-dopa exposure. Second, we show here for the first time that astrocytes play a crucial role in this response. Not only was VEGF abundantly expressed in astrocytic cell bodies and processes, but also dopamine and D1 receptor stimulation were found to induce VEGF messenger RNA in isolated astrocytes. Our findings of astrocytic VEGF expression are in agreement with results reported from a variety of pathophysiological conditions (Araneda *et al*., 2008; Nicoletti *et al*., 2008; Barouk *et al*., 2011; Saito *et al*., 2011). Although VEGF can be expressed in microglia under conditions of neuroinflammatory activation (Tran *et al*., 2005; Ryu *et al*., 2009), we did not observe any co-localization of VEGF with markers of resting or activated microglia, consistent with the absence of significant microglial activation in either the striatum or the substantia nigra pars reticulata in our animal models of Parkinson's disease and LID (Westin *et al*., 2006; Lindgren *et al*., 2007; and present study, see Supplementary Fig. 3). Previous studies have shown that astrocytes in the striatum express high levels of D1- and D2-type receptors, which would make them more responsive to dopamine than astrocytes in other brain regions (Hansson *et al*., 1984; Zanassi *et al*., 1999; Miyazaki *et al*., 2004). Accordingly, in our *in vitro* assay, the induction of VEGF messenger RNA by a D1-class receptor agonist was 2-fold larger in striatal than cortical astrocytes. In contrast, the stimulation of D2-class receptors had no effect on VEGF messenger RNA, which was instead induced by D2 receptor antagonism. These results show an interesting concordance with a pharmacological study using the rat model of LID, in which L-dopa-induced endothelial proliferation was potentiated by the co-administration of a D2 receptor antagonist (Lindgren *et al*., 2009). Moreover, our findings are in keeping with the reported anti-angiogenic effects of D2 receptor stimulation, which has been shown to reduce VEGF expression and antagonize VEGFR2 activation in cultured endothelial cells and in endocrine organs (Basu *et al*., 2001; Sarkar *et al*., 2004; Cristina *et al*., 2005). In line with our previous pharmacological investigations (Lindgren *et al*., 2009), the present results thus point to a critical role of D1 receptors in L-dopa-induced angiogenesis and raise a previously unappreciated role of this

receptor class; namely, the stimulation of VEGF gene expression in astrocytes. A direct stimulation of astrocytic D1-like receptors following L-dopa administration cannot, however, explain the anatomical distribution of the angiogenic response, which is most pronounced in the basal ganglia output stations (substantia nigra pars reticulata, and entopeduncular nucleus/internal globus pallidus), followed by the external globus pallidus and the caudate–putamen (Westin *et al*., 2006). Regional differences also occur within the caudate–putamen itself, since the largest extents of endothelial proliferation, nestin upregulation and increased blood–brain barrier permeability occur in its lateral quadrants at mid-caudal levels (Westin *et al*., 2006). It is therefore likely that astrocytes are more affected in certain regions not because of their relative abundance of D1 receptors, but because of the specific neurochemical imbalances that underlie LID. In particular, both the lateral striatum and the substantia nigra pars reticulata show large increases in extracellular dopamine and glutamate levels following the administration of L-dopa and these changes are significantly larger, or exclusively seen, in dyskinetic animals (Robelet *et al*., 2004; Mela *et al*., 2007; Lindgren *et al*., 2010).

The antidyskinetic and antiangiogenic effects of the high-affinity VEGFR2 antagonist, vandetanib (Experiment 3) indicate that a VEGF-dependent angiogenic activity causally contributes to the development of LID. Although having greatest affinity for VEGFR2, vandetanib may also affect signalling downstream of the epidermal growth factor receptor and glial cell line-derived neurotrophic factor receptor, RET (Wedge *et al*., 2002; Ryan *et al*., 2005). These additional actions are, however, unlikely to explain the effects of vandetanib in the present study. Indeed, we are not aware of any angiogenic effects produced by the GDNF family of ligands, and any possible anti-angiogenic effect of EGFR antagonism would depend on its impact on VEGF expression and signalling (Larsen *et al*., 2011). An important suggestion provided by the vandetanib study is that antagonizing VEGF can reduce dyskinesia only under conditions of high angiogenic stimulation. Indeed, the compound did not produce any clear-cut effect when animals were treated with the lower dose of L-dopa (6 mg/kg/day), and its antidyskinetic properties were revealed by increasing the L-dopa dose, first to 12 and then to 24 mg/kg/day. Thus, while not being a necessary requirement for LID to occur, angiogenic activity and microvascular remodelling should be seen as an exacerbating factor whose weight increases during the course of Parkinson's disease in parallel with a larger cumulative exposure to L-dopa.

The functional implications of angiogenesis in Parkinson's disease and LID remain to be determined but are likely to be biologically significant. To the extent that newly formed vessels are perfused, an increased vessel density would drive more blood flow to the affected brain regions. An elegant PET study has investigated the coupling between cerebral metabolic rate and cerebral blood flow in patients with Parkinson's disease, who were scanned in the 'ON' and 'OFF' L-dopa condition (Hirano *et al*., 2008). A strong dissociation between cerebral metabolic rate and cerebral blood flow was found in the putamen and the globus pallidus 'ON' L-dopa due to a large increase in regional cerebral blood flow. Interestingly, the magnitude of this effect was extremely pronounced in patients with Parkinson's disease affected by dyskinesia. These findings are in line with previous reports of abnormal cerebral blood flow responses to L-dopa therapy, which also pointed to an association with disease progression and with the development of dyskinesia (Hershey *et al*., 1998). An increase in regional cerebral blood flow 'ON' L-dopa is likely to be triggered by an elevation of extracellular dopamine levels. Indeed, dopamine can cause concentration-dependent vasodilation in cerebral blood vessels (Edvinsson *et al*., 1978; Iadecola *et al*., 1998; Krimer *et al*., 1998). Moreover, studies in both patients with Parkinson's disease and rat models of Parkinson's disease have shown significantly larger increases in extracellular dopamine levels in dyskinetic individuals compared to non-dyskinetic cases following the administration of L-dopa (de la Fuente-Fernandez *et al*., 2004; Meissner *et al*., 2006; Pavese *et al*., 2006; Lindgren *et al*., 2010). Along with acute haemodynamic effects, high and fluctuating levels of dopamine may also promote endothelial proliferation and angiogenic activity through shear stress on vessel walls (Schierling *et al*., 2009) and induction of VEGF in astrocytes (this study). Large intermittent elevations of extracellular dopamine levels during L-dopa pharmacotherapy may therefore trigger a vicious circle of increases in regional cerebral blood flow and angiogenesis, which may in turn affect the blood–brain barrier (Johansson *et al*., 1977; Hardebo *et al*., 1980; Nag *et al*., 2002, 2009). In turn, an altered function of the blood–brain barrier is the most plausible mechanism linking angiogenesis to LID. We have previously hypothesized that increased blood–brain barrier permeability alters the passage of L-dopa from blood to brain, resulting in higher brain levels of L-dopa in dyskinetic animals (Westin *et al*., 2006). This suggestion is in line with the results of Carta *et al*. (2006), but not with a more recent study, in which striatal and nigral levels of L-dopa did not differ significantly between dyskinetic and non-dyskinetic rats (Lindgren *et al*., 2010). Independent of its effect on central L-dopa levels, an increased blood–brain barrier permeability may, however, contribute to LID through its impact on the extracellular milieu. Indeed, unregulated influx of ions and plasma constituents through a leaky blood–brain barrier can pose a challenge to the astrocytic clearance capacity (Nedergaard *et al*., 2010) and produce foci of increased neuronal excitability, similar to the situation described in experimental models of epilepsy (Ivens *et al*., 2007; van Vliet *et al*., 2007; Nicoletti *et al*., 2008). A recent study in dyskinetic macaques failed to detect alterations in blood–brain barrier permeability using contrast-based MRI (Astradsson *et al*., 2009), but this study was performed in anaesthetized animals at an undefined interval from the last L-dopa dose, probably lacking the stimuli required to recruit angiogenic vessels, which are mainly perfused under conditions of increased blood flow (Vogel *et al*., 2004).

This study has provided new evidence about the role and regulation of VEGF in the L-dopa-treated parkinsonian brain. We propose that VEGF-dependent microvascular plasticity contributes to the chronicity of LID in the advanced stages of Parkinson's disease and that it may also contribute to individual variations in the severity of this movement disorder. Protective therapies targeting the vasoactive response to L-dopa may stabilize the microvasculature and prevent the worsening of dyskinesia over time. Longitudinal studies on patients with Parkinson's disease using a combination of clinical assessments, wet biomarkers and

functional imaging approaches will be required to provide definite support for this notion.

Acknowledgements

The authors are thankful to Ann-Christin Lindh and Michael Sparrenius for excellent technical assistance. HBTRC at McLean Hospital, Harvard Medical School, Belmont, MA, USA, and Linda Parsons at the Queen Square Brain Bank, London, UK for providing tissue. Dr Ryan Anderson and Dr Paul Elvin at Astra Zeneca, Alderley Park, UK, for providing vandetanib and related pharmacokinetic/pharmacodynamic information. Dr Diether Lambrechts and Prof Peter Carmeliet (Katholieke University, Leuven, Belgium), Dr Annette Persson and Assoc. Prof. Elisabet Englund (Department of Pathology in Lund, Sweden) for their support and helpful discussions.

Funding

The research leading to these results have been funded by: The Michael J Fox Foundation of Parkinson's Disease Research (to M.A.C.); the Swedish Research Council (to M.A.C.); the Swedish Lundbeck Foundation (to H.S.L.); European Community's Seventh Framework Programme (FP7/2007-2013) [grant number 215618 (2008) to M.A.C.]; National Institutes of Health (grants NS48235 to C.K.; MH068855 to HBTRC; T32MH064913 to S.E.S.); and a subcontract from The NIH Morris K. Udall Center of Excellence for Parkinson's Disease Research (NIH P50 NS071675 to M.A.C.).

Supplementary material

Supplementary material is available at *Brain* online.

References

Araneda S, Commin L, Atlagich M, Kitahama K, Parraguez VH, Pequignot J-M, et al. VEGF overexpression in the astroglial cells of rat brainstem following ozone exposure. Neurotoxicology 2008; 29: 920–7.

Astradsson A, Jenkins BG, Choi JK, Hallett PJ, Levesque MA, McDowell JS, et al. The blood-brain barrier is intact after levodopa-induced dyskinesias in parkinsonian primates–evidence from in vivo neuroimaging studies. Neurobiol Dis 2009; 35: 348–51.

Attwell D, Buchan AM, Charpak S, Lauritzen M, Macvicar BA, Newman EA. Glial and neuronal control of brain blood flow. Nature 2010; 468: 232–43.

Barcia C, Bautista V, Sanchez-Bahillo A, Fernandez-Villalba E, Faucheux B, Poza YPM, et al. Changes in vascularization in substantia nigra pars compacta of monkeys rendered parkinsonian. J Neural Transm 2005; 112: 1237–48.

Barouk S, Hintz T, Li P, Duffy AM, Maclusky NJ, Scharfman HE. 17{beta}-Estradiol Increases Astrocytic Vascular Endothelial Growth Factor (VEGF) in Adult Female Rat Hippocampus. Endocrinology 2011; 152: 1745–51.

Bartels AL, Willemsen AT, Kortekaas R, de Jong BM, de Vries R, de Klerk O, et al. Decreased blood-brain barrier P-glycoprotein function in the progression of Parkinson's disease, PSP and MSA. J Neural Transm 2008; 115: 1001–9.

Basu S, Nagy JA, Pal S, Vasile E, Eckelhoefer IA, Bliss VS, et al. The neurotransmitter dopamine inhibits angiogenesis induced by vascular permeability factor/vascular endothelial growth factor. Nat Med 2001; 7: 569–74.

Bauer AT, Bürgers HF, Rabie T, Marti HH. Matrix metalloproteinase-9 mediates hypoxia-induced vascular leakage in the brain via tight junction rearrangement. J Cereb Blood Flow Metab 2010; 30: 837–48.

Black JE, Isaacs KR, Anderson BJ, Alcantara AA, Greenough WT. Learning causes synaptogenesis, whereas motor activity causes angiogenesis, in cerebellar cortex of adult rats. Proc Natl Acad Sci USA 1990; 87: 5568–72.

Braak H, Braak E. Neuropathological stageing of Alzheimer-related changes. Acta Neuropathol 1991; 82: 239–59.

Calabresi P, Di Filippo M, Ghiglieri V, Picconi B. Molecular mechanisms underlying levodopa-induced dyskinesia. Mov Disord 2008; 23 (Suppl 3): S570–9.

Carmeliet P. Mechanisms of angiogenesis and arteriogenesis. Nature Med 2000; 6: 389–95.

Carta M, Lindgren HS, Lundblad M, Stancampiano R, Fadda F, Cenci MA. Role of striatal L-DOPA in the production of dyskinesia in 6-hydroxydopamine lesioned rats. J Neurochem 2006; 96: 1718–27.

Carvey PM, Zhao CH, Hendey B, Lum H, Trachtenberg J, Desai BS, et al. 6-Hydroxydopamine-induced alterations in blood-brain barrier permeability. Eur J Neurosci 2005; 22: 1158–68.

Cavaglia M, Dombrowski SM, Drazba J, Vasanji A, Bokesch PM, Janigro D. Regional variation in brain capillary and vascular response to ischemia. Brain Res 2001; 81–93.

Cenci MA, Lee CS, Bjorklund A. L-DOPA-induced dyskinesia in the rat is associated with striatal overexpression of prodynorphin- and glutamic acid decarboxylase mRNA. Eur J Neurosci 1998; 10: 2694–706.

Cenci MA, Lundblad M. Ratings of L-DOPA-induced dyskinesia in the unilateral 6-OHDA lesion model of Parkinson's disease in rats and mice. Current protocols in neuroscience / editorial board, Jacqueline N Crawley [et al. 2007;Chapter 9:Unit 9 25.

Cenci MA, Ohlin KE, Rylander D. Plastic effects of L-DOPA treatment in the basal ganglia and their relevance to the development of dyskinesia. Parkinsonism Relat Disord 2009; 15 (Suppl 3): S59–63.

Chmelova J, Kolar Z, Prochazka V, Curik R, Dvorackova J, Sirucek P, et al. Moyamoya disease is associated with endothelial activity detected by anti-nestin antibody. Biomed Pap Med Fac Univ Palacky Olomouc Czech Repub 2010; 154: 159–62.

Cristina C, Diaz-Torga G, Baldi A, Gongora A, Rubinstein M, Low MJ, et al. Increased pituitary vascular endothelial growth factor-a in dopaminergic D2 receptor knockout female mice. Endocrinology 2005; 146: 2952–62.

Croll SD, Ransohoff RM, Cai N, Zhang Q, Martin FJ, Wei T, et al. VEGF-mediated inflammation precedes angiogenesis in adult brain. Exp Neurol 2004; 187: 388–402.

de la Fuente-Fernandez R, Sossi V, Huang Z, Furtado S, Lu JQ, Calne DB, et al. Levodopa-induced changes in synaptic dopamine levels increase with progression of Parkinson's disease: implications for dyskinesias. Brain 2004; 127 (Pt 12): 2747–54.

Ding YH, Li J, Zhou Y, Rafols JA, Clark J. Cerebral angiogenesis and expression of angiogenic factors in aging rats after exercise. Current Neurovasc Res 2006; 3: 15–23.

Edvinsson L, Hardebo JE, McCulloch J, Owman C. Vasomotor response of cerebral blood vessels to dopamine and dopaminergic agonists. Adv Neurol 1978; 20: 85–96.

Farkas E, De Jong GI, de Vos RA, Jansen Steur EN, Luiten PG. Pathological features of cerebral cortical capillaries are doubled in Alzheimer's disease and Parkinson's disease. Acta Neuropathol 2000; 100: 395–402.

Faucheux BA, Bonnet AM, Agid Y, Hirsch EC. Blood vessels change in the mesencephalon of patients with Parkinson's disease. Lancet 1999; 353: 981–2.

Ferrara N. Vascular endothelial growth factor: molecular and biological aspects. Curr Top Microbiol Immunol 1999; 237: 1–30.

Gibb WR, Lees AJ. The relevance of the Lewy body to the pathogenesis of idiopathic Parkinson's disease. J Neurol Neurosurg Psychiatry 1988; 51: 745–52.

Gomez R, Gonzalez-Izquierdo M, Zimmermann RC, Novella-Maestre E, Alonso-Muriel I, Sanchez-Criado J, et al. Low-dose dopamine agonist administration blocks vascular endothelial growth factor (VEGF)-mediated vascular hyperpermeability without altering VEGF receptor 2-dependent luteal angiogenesis in a rat ovarian hyperstimulation model. Endocrinology 2006; 147: 5400–11.

Gustafson DL, Bradshaw-Pierce EL, Merz AL, Zirrolli JA. Tissue distribution and metabolism of the tyrosine kinase inhibitor ZD6474 (Zactima) in tumor-bearing nude mice following oral dosing. J Pharmacol Exp Ther 2006; 318: 872–80.

Hansson E, Ronnback L, Sellstrom A. Is there a 'dopaminergic glial cell'? Neurochem Res 1984; 9: 679–89.

Hardebo JE, Nilsson B. Hemodynamic changes in brain caused by local infusion of hyperosomolar solutions, in particular relation to blood-brain barrier opening. Brain Res 1980; 181: 49–59.

Hawkins BT, Sykes DB, Miller DS. Rapid, reversible modulation of blood-brain barrier P-glycoprotein transport activity by vascular endothelial growth factor. J Neurosci 2010; 30: 1417–25.

Hershey T, Black KJ, Stambuk MK, Carl JL, McGee-Minnich LA, Perlmutter JS. Altered thalamic response to levodopa in Parkinson's patients with dopa-induced dyskinesias. Proc Natl Acad Sci USA 1998; 95: 12016–21.

Hirano S, Asanuma K, Ma Y, Tang C, Feigin A, Dhawan V, et al. Dissociation of metabolic and neurovascular responses to levodopa in the treatment of Parkinson's disease. J Neurosci 2008; 28: 4201–9.

Huot P, Johnston TH, Koprich JB, Winkelmolen L, Fox SH, Brotchie JM. Regulation of cortical and striatal 5-HT(1 A) receptors in the MPTP-lesioned macaque. Neurobiol Aging 2010.

Iadecola C. Neurogenic control of the cerebral microcirculation: is dopamine minding the store? Nat Neurosci 1998; 1: 263–5.

Iadecola C. Neurovascular regulation in the normal brain and in Alzheimer's disease. Nat Rev Neurosci 2004; 5: 347–60.

Ivens S, Kaufer D, Flores LP, Bechmann I, Zumsteg D, Tomkins O, et al. TGF-beta receptor-mediated albumin uptake into astrocytes is involved in neocortical epileptogenesis. Brain 2007; 130 (Pt 2): 535–47.

Johansson B, Nilsson B. The pathophysiology of the blood-brain barrier dysfunction induced by severe hypercapnia and by epileptic brain activity. Acta Neuropathol 1977; 38: 153–8.

Kalaria RN, Kroon SN. Expression of leukocyte antigen CD34 by brain capillaries in Alzheimer's disease and neurologically normal subjects. Acta Neuropathol 1992; 84: 606–12.

Konradi C, Westin JE, Carta M, Eaton ME, Kuter K, Dekundy A, et al. Transcriptome analysis in a rat model of L-DOPA-induced dyskinesia. Neurobiol Dis 2004; 17: 219–36.

Kortekaas R, Leenders KL, van Oostrom JC, Vaalburg W, Bart J, Willemsen AT, et al. Blood-brain barrier dysfunction in parkinsonian midbrain in vivo. Ann Neurol 2005; 57: 176–9.

Krimer LS, Muly EC, Williams GV, Goldman-Rakic PS. Dopaminergic regulation of cerebral cortical microcirculation. Nat Neurosci 1998; 1: 286–9.

Krum JM, Mani N, Rosenstein JM. Angiogenic and astroglial responses to vascular endothelial growth factor administration in adult rat brain. Neuroscience 2002; 110: 589–604.

Larrivee B, Karsan A. Signaling pathways induced by vascular endothelial growth factor (Review). Int J Mol Med 2000; 5: 447–56.

Larsen AK, Ouaret D, El Ouadrani K, Petitprez A. Targeting EGFR and VEGF(R) pathway cross-talk in tumor survival and angiogenesis. Pharmacol Therapeutics 2011; 131: 80–90.

Lindgren HS, Rylander D, Ohlin KE, Lundblad M, Cenci MA. The 'motor complication syndrome' in rats with 6-OHDA lesions treated chronically with L-DOPA: relation to dose and route of administration. Behav Brain Res 2007; 177: 150–9.

Lindgren HS, Ohlin KE, Cenci MA. Differential involvement of D1 and D2 dopamine receptors in L-DOPA-induced angiogenic activity in a rat model of Parkinson's disease. Neuropsychopharmacology 2009; 34: 2477–88.

Lindgren HS, Andersson DR, Lagerkvist S, Nissbrandt H, Cenci MA. L-DOPA-induced dopamine efflux in the striatum and the substantia nigra in a rat model of Parkinson's disease: temporal and quantitative relationship to the expression of dyskinesia. J Neurochem 2010; 112: 1465–76.

Little KY, Carroll FI, Cassin BJ. Characterization and localization of [125I]RTI-121 binding sites in human striatum and medial temporal lobe. J Pharmacol Exp Ther 1995; 274: 1473–83.

Lundblad M, Andersson M, Winkler C, Kirik D, Wierup N, Cenci MA. Pharmacological validation of behavioural measures of akinesia and dyskinesia in a rat model of Parkinson's disease. Eur J Neurosci 2002; 15: 120–32.

Mai JK, Paxinos AJ. Atlas of the human brain. 2nd edn. Elsevier Academic Press; 2004.

Mani N, Khaibullina A, Krum JM, Rosenstein JM. Activation of receptor-mediated angiogenesis and signaling pathways after VEGF administration in fetal rat CNS explants. J Cereb Blood Flow Metab 2003; 23: 1420–9.

Manson A, Schrag A. Levodopa-induced dyskinesias, the clinical problem: clinical features, incidence, risk factors, management and impact on quality of life. In: Bezard E, editor. Recent breakthroughs in basal ganglia research. New York, NY: Nova Science Publishers Inc.; 2006. p. 369–80.

Marti HJ, Bernaudin M, Bellail A, Schoch H, Euler M, Petit E, et al. Hypoxia-induced vascular endothelial growth factor expression precedes neovascularization after cerebral ischemia. Am J Pathol 2000; 156: 965–76.

McKeith IG, Galasko D, Kosaka K, Perry EK, Dickson DW, Hansen LA, et al. Consensus guidelines for the clinical and pathologic diagnosis of dementia with Lewy bodies (DLB): report of the consortium on DLB international workshop. Neurology 1996; 47: 1113–24.

Meissner W, Ravenscroft P, Reese R, Harnack D, Morgenstern R, Kupsch A, et al. Increased slow oscillatory activity in substantia nigra pars reticulata triggers abnormal involuntary movements in the 6-OHDA-lesioned rat in the presence of excessive extracellular striatal dopamine. Neurobiol Dis 2006; 22: 586–98.

Mela F, Marti M, Dekundy A, Danysz W, Morari M, Cenci MA. Antagonism of metabotropic glutamate receptor type 5 attenuates l-DOPA-induced dyskinesia and its molecular and neurochemical correlates in a rat model of Parkinson's disease. J Neurochem 2007; 101: 483–97.

Mele T, Carman-Krzan M, Juric DM. Regulatory role of monoamine neurotransmitters in astrocytic NT-3 synthesis. Int J Dev Neurosci 2010; 28: 13–9.

Miyazaki I, Asanuma M, Diaz-Corrales FJ, Miyoshi K, Ogawa N. Direct evidence for expression of dopamine receptors in astrocytes from basal ganglia. Brain Res 2004; 1029: 120–3.

Mokry J, Nemeneck S. Cerebral angiogenesis shows nestin expression in endothelial cells. Gen Physiolo Biophys 1999; 18 (Suppl 1): 25–9.

Mokrý J, Cízková D, Filip S, Ehrmann J, Osterreicher J, Kolár Z, et al. Nestin expression by newly formed human blood vessels. Stem Cells Dev 2004; 13: 658–64.

Nag S. The blood-brain barrier and cerebral angiogenesis: lessons from the cold-injury model. Trends Mol Med 2002; 8: 38–44.

Nag S, Manias JL, Stewart DJ. Pathology and new players in the pathogenesis of brain edema. Acta Neuropathol 2009; 118: 197–217.

Naydenov AV, Vassoler F, Luksik AS, Kaczmarska J, Konradi C. Mitochondrial abnormalities in the putamen in Parkinson's disease dyskinesia. Acta Neuropathol 2010; 120: 623–31.

Nedergaard M, Rodríguez JJ, Verkhratsky A. Glial calcium and diseases of the nervous system. Cell Calcium 2010; 47: 140–9.

Nicoletti JN, Shah SK, McCloskey DP, Goodman JH, Elkady A, Atassi H, et al. Vascular endothelial growth factor is upregulated after status epilepticus and protects against seizure-induced neuronal loss in hippocampus. Neuroscience 2008; 151: 232–41.

Ohta K, Kuno S, Mizuta I, Fujinami A, Matsui H, Ohta M. Effects of dopamine agonists bromocriptine, pergolide, cabergoline, and SKF-38393 on GDNF, NGF, and BDNF synthesis in cultured mouse astrocytes. Life Sci 2003; 73: 617–26.

Pavese N, Evans AH, Tai YF, Hotton G, Brooks DJ, Lees AJ, et al. Clinical correlates of levodopa-induced dopamine release in Parkinson disease: a PET study. Neurology 2006; 67: 1612–7.

Perea G, Navarrete M, Araque A. Tripartite synapses: astrocytes process and control synaptic information. Trends Neurosci 2009; 32: 421–31.

Picconi B, Ghiglieri V, Bagetta V, Barone I, Sgobio C, Calabresi P. Striatal synaptic changes in experimental parkinsonism: role of NMDA receptor trafficking in PSD. Parkinsonism Relat Disord 2008; 14 (Suppl 2): S145–9.

Rigau V, Morin M, Rousset M-C, de Bock F, Lebrun A, Coubes P, et al. Angiogenesis is associated with blood-brain barrier permeability in temporal lobe epilepsy. Brain 2007; 130 (Pt 7): 1942–56.

Robelet S, Melon C, Guillet B, Salin P, Kerkerian-Le Goff L. Chronic L-DOPA treatment increases extracellular glutamate levels and GLT1 expression in the basal ganglia in a rat model of Parkinson's disease. Eur J Neurosci 2004; 20: 1255–66.

Robertson GS, Robertson HA. Evidence that L-dopa-induced rotational behavior is dependent on both striatal and nigral mechanisms. J Neurosci 1989; 9: 3326–31.

Rosenstein JM, Mani N, Silverman WF, Krum JM. Patterns of brain angiogenesis after vascular endothelial growth factor administration in vitro and in vivo. Proc Natl Acad Sci USA 1998; 95: 7086–91.

Rosenstein JM, Krum JM. New roles for VEGF in nervous tissue–beyond blood vessels. Exp Neurol 2004; 187: 246–53.

Ryan AJ, Wedge SR. ZD6474–a novel inhibitor of VEGFR and EGFR tyrosine kinase activity. Br J Cancer 2005; 92 (Suppl 1): S6–13.

Ryu JK, Cho T, Choi HB, Wang YT, Mclarnon JG. Microglial VEGF receptor response is an integral chemotactic component in Alzheimer's disease pathology. J Neurosci 2009; 29: 3–13.

Saito T, Shibasaki K, Kurachi M, Puentes S, Mikuni M, Ishizaki Y. Cerebral capillary endothelial cells are covered by the VEGF-expressing foot processes of astrocytes. Neurosci Lett 2011; 497: 116–21.

Sarkar C, Chakroborty D, Mitra RB, Banerjee S, Dasgupta PS, Basu S. Dopamine in vivo inhibits VEGF-induced phosphorylation of VEGFR-2, MAPK, and focal adhesion kinase in endothelial cells. Am J Physiol Heart Circ Physiol 2004; 287: H1554–60.

Schallert T, Fleming SM, Leasure JL, Tillerson JL, Bland ST. CNS plasticity and assessment of forelimb sensorimotor outcome in unilateral rat models of stroke, cortical ablation, parkinsonism and spinal cord injury. Neuropharmacology 2000; 39: 777–87.

Schierling W, Troidl K, Mueller C, Troidl C, Wustrack H, Bachmann G, et al. Increased intravascular flow rate triggers cerebral arteriogenesis. J Cereb Blood Flow Metab 2009; 29: 726–37.

Schmid-Brunclik N, Burgi-Taboada C, Antoniou X, Gassmann M, Ogunshola OO. Astrocyte responses to injury: VEGF simultaneously modulates cell death and proliferation. AJP: Regul Integr Comp Physiol 2008; 295: R864–73.

Swain RA, Harris AB, Wiener EC, Dutka MV, Morris HD, Theien BE, et al. Prolonged exercise induces angiogenesis and increases cerebral blood volume in primary motor cortex of the rat. Neuroscience 2003; 117: 1037–46.

Tran KC, Ryu JK, McLarnon JG. Induction of angiogenesis by platelet-activating factor in the rat striatum. Neuroreport 2005; 16: 1579–83.

van Vliet EA, da Costa Araujo S, Redeker S, van Schaik R, Aronica E, Gorter JA. Blood-brain barrier leakage may lead to progression of temporal lobe epilepsy. Brain 2007; 130 (Pt 2): 521–34.

Vogel J, Gehrig M, Kuschinsky W, Marti HH. Massive Inborn Angiogenesis in the Brain Scarcely Raises Cerebral Blood Flow. J Cereb Blood Flow Metab 2004; 849–59.

Voon V, Fernagut PO, Wickens J, Baunez C, Rodriguez M, Pavon N, et al. Chronic dopaminergic stimulation in Parkinson's disease: from dyskinesias to impulse control disorders. Lancet Neurol 2009; 8: 1140–9.

Wada K, Arai H, Takanashi M, Fukae J, Oizumi H, Yasuda T, et al. Expression levels of vascular endothelial growth factor and its receptors in Parkinson's disease. Neuroreport 2006; 17: 705–9.

Wedge SR, Ogilvie DJ, Dukes M, Kendrew J, Chester R, Jackson JA, et al. ZD6474 inhibits vascular endothelial growth factor signaling, angiogenesis, and tumor growth following oral administration. Cancer Res 2002; 62: 4645–55.

Westin JE, Lindgren HS, Gardi J, Nyengaard JR, Brundin P, Mohapel P, et al. Endothelial proliferation and increased blood-brain barrier permeability in the basal ganglia in a rat model of 3,4-dihydroxyphenyl-L-alanine-induced dyskinesia. J Neurosci 2006; 26: 9448–61.

Winkler C, Kirik D, Bjorklund A, Cenci MA. L-DOPA-induced dyskinesia in the intrastriatal 6-hydroxydopamine model of Parkinson's disease: relation to motor and cellular parameters of nigrostriatal function. Neurobiol Dis 2002; 10: 165–86.

Zanassi P, Paolillo M, Montecucco A, Avvedimento EV, Schinelli S. Pharmacological and molecular evidence for dopamine D(1) receptor expression by striatal astrocytes in culture. J Neurosci Res 1999; 58: 544–52.

Zhang ZG, Zhang L, Jiang Q, Zhang R, Davies K, Powers C, et al. VEGF enhances angiogenesis and promotes blood-brain barrier leakage in the ischemic brain. J Clin Invest 2000; 106: 829–38.

Zlokovic BV. The blood-brain barrier in health and chronic neurodegenerative disorders. Neuron 2008; 57: 178–201.